Effect of dislocation density evolution on the thermomechanical response of metals with different crystal structures at low and high strain rates and temperatures

G. Z. VOYIADJIS, F. H. ABED

Department of Civil and Environmental Engineering
Louisiana State University,
Baton Rouge, LA 70803 USA

THE CONTRIBUTION of plastic strain evolution of mobile and forest dislocation densities to the thermal and athermal components of polycrystalline metals flow stress is investigated in this work. The thermomechanical response is characterized here for body centered cubic (bcc), face centered cubic (fcc) and hexagonal close-packed (hcp) structures of metals at low and high strain rates and temperatures. Consequently, the simulation of the plastic flow stress for these metals is developed based on the concept of thermal activation energy, the additive decomposition of the flow stress, dislocations interaction mechanisms and the role of dislocations dynamic in crystals. The material parameters of the proposed modeling are physically defined and related to the nano- and micro-structure quantities. On the other hand, the hardening parameters of each kind of metal structures are presented in two different forms; physically based definition which is developed, based on the aforementioned concepts and empirical relation which is used by several authors and is based on experimental observations. Several experimental data obtained by different authors for Niobium, Tantalum, Vanadium, Oxygen Free High Conductivity (OFHC) Copper, and Titanium are used in evaluating the proposed models. Good correlation is observed between the proposed models predictions and the experimental observations. Moreover, the predicted results show that the effect of mobile and forest dislocation densities evolution with plastic strain on the thermal stress of bcc metals is almost negligible and pertained totally to the athermal stress part, whereas the plastic strain evolution of these dislocation densities play crucial roles in determining the plastic thermal flow stress of most fcc metals. The thermal and athermal flow stresses for hcp metals, however, show a behavior that is a combination of that for both bcc and fcc plastic deformation models.

Key words: plasticity, mobile and forest dislocation density, plastic flow stress, activation energy analysis, thermomechanical response; activation energy, plasticity.

1. Introduction

THE PLASTIC FLOW STRESS for relatively pure metals is determined through the interaction of dislocations, which are moving inside the crystal lattice, with the lattice itself and with the available barriers encountered inside the lattice. ASHBY and FROST [4] pointed out that dislocation motion through the lattice

or past an obstacle require surmounting of the energy barrier by a combination of applied stress and thermal activation. Thus, at the microscale level, the mechanisms associated with dislocation motion and dislocation multiplication, the statistics of mobile dislocation populations, the nature and the statistics of obstacle distributions and the relationship between the externally imposed plastic strain rate and the dislocation kinetics, determine the form of the macroscopic plastic response. Moreover, the crystal lattice configuration plays a crucial role in determining the effect of thermal activation on the mechanical response of relatively pure metals which are mainly classified into three common crystal types; body-centered cubic (bcc), face-centered cubic (fcc) and hexagonal-close-packed (hcp). Each of these three crystal structures exhibits a characteristic thermomechanical behavior which is associated with the available slip systems and symmetries as well as with the nature of dislocation cores. Good reviews of plastic deformation in different crystal structure types of metals are provided by Kubin [30], Christian [14], Taylor [53], Vitek and Duesbury [54], Chichili et al. [13], Nemat-Nasser et al. [44] and Lennon and Ramesh [33].

A great deal of effort has been made in understanding the influence of temperature and strain rate on the flow stress of different structure types of metals. This understanding, however, is essential for the modeling and analysis of numerous processes including high-speed machining, impact, penetration and shear localization. Recently, considerable progress has been made in understanding the role of rate controlling dislocation mechanisms on the temperature and strain rate dependence of the flow stress for metals and alloys. Hoge and Murkherjee [18] studied the effect of both temperature and strain rates on the lower yield stress of tantalum as a bcc metal and proposed a model incorporating the combined operation of the Peierls' mechanism and dislocation drag process. Zerilli and Armstrong [59] used dislocation mechanics concept to develop a constitutive model that accounts for strain, strain rate and temperature in a coupled manner, which can be incorporated in computer codes for applications related to dynamic loading conditions. Their model considers two different forms for the two different classes of metals (bcc and fcc). The rational for the differences in the two forms mainly depends on the dislocation characteristics for each particular structure. Bcc metals show stronger dependence of the yield stress on temperature and strain rate while in the case of fcc metals the yield stress is mainly affected by strain hardening. In other words, the cutting of dislocation forests is the principal mechanism in fcc metals, while in bcc metals; the overcoming of Peierls-Nabarro barriers is the principal mechanism. Zerilli–Armstrong (Z–A) model has been derived based on the concept of thermal activation analysis for overcoming local obstacles to dislocation motion. This model has been widely used in many computer codes from which its material parameters, as first believed, are physically interpreted. Very recently, Voyiadjis and Abed [55]) explained that the phys-

ical definitions of the Z–A model parameters are, in fact, not accurate because of the assumption made by using the expansion $\ln(1 + x) \simeq x$ in the model derivation. This expansion, however, is valid only for values $x \ll 1.0$, whereas the definition of the variable x given by Z–A model indicates that its numerical value increases and approaches the value of one with strain rate and temperature increase. This, in turn, makes the Z–A parameters lose their physical meaning when they are used in high temperature and strain rate applications. In other words, by using the above-mentioned expansion, the Z–A model derivation was directed to match the experimental evidence which shows that the temperature degradation of the flow stress can be fitted using an exponential form (see the paper of VOYIADJIS and ABED [55] for more details).

KLEPACZKO [25, 26] derived a constitutive model that is based on a consistent approach to the kinetics of macroscopic plastic flow of metals with bcc and fcc structures. His constitutive formalism was applied utilizing one state variable which is the total dislocation density and assuming that plastic deformation in shear is the fundamental mode in metal plasticity. Furthermore, he assumed that at constant microstructure, the flow stress consists of two components: the internal stress and the effective stress. The internal stress is developed by the long-range strong obstacles to dislocation motion whereas the effective stress is due to thermally activated short-range obstacles. Unlike most experimental observations and theoretical interpretations, Klepaczko pointed out that for certain bcc or fcc metals, athermal and thermal flow stress components that are pertained to the resistance of long and short range barriers respectively are strain rate and temperature-dependent. Klepaczko and his co-workers (KLEPACZKO and REZAIG [27] and RUSINEK and KLEPACZKO [48]) have successfully evaluated the material parameters of the derived constitutive model for different bcc and fcc metals and they were able to study the adiabatic shear banding in mild steel numerically.

Nemat-Nasser and his co-workers (e.g., NEMAT-NASSER and ISAACS, [41], NEMAT-NASSER and LI [42] NEMAT-NASSER *et al.* [43] and NEMAT-NASSER and GUO [44, 45]) developed an experimental technique measuring the flow stress of different bcc, fcc and hcp metals and alloys over a broad range of strains, strain rate and temperatures in uniaxial compression. Some of their experimental results are, actually, used in this work for models evaluation and comparisons. They also presented a constitutive model that characterizes the plastic deformation of different metals and alloys using the thermal activation concept and assuming constant dislocation density throughout the deformation process. That is neither the plastic strain evolution of dislocation density nor the rate multiplication of the dislocation density evolution is considered.

VOYIADJIS and ABED [55] incorporated the production rate of dislocation density in modeling the plastic flow stress for both bcc and fcc metals using

the concept of thermal activation analysis as well as the dislocation interaction mechanisms. Some of their models parameters are physically derived and related to the micro-structural quantities. Others, on the other hand, are defined empirically based on the experimental results. It was concluded that the contribution of mobile dislocation density rate to the plastic deformation modeling shows considerable effect on the prediction of the flow stress, particularly in the case of high strain rates and temperatures. Furthermore, Abed and Voyiadjis [1] used a combination of their bcc and fcc models in characterizing the thermomechanical behavior of AL-6XN stainless steel over a wide range of temperatures and strain rates.

In this paper, the effect of plastic strain evolution of dislocation density is utilized in determining the plastic flow stress of three major categories of metal structures: body centered cubic (bcc), face centered cubic (fcc), and hexagonal close packed (hcp) over a wide range of temperatures and strain rates. The proposed constitutive models are derived based on the concept of thermal activation analysis, dislocation interaction mechanisms, experimental observations, and the additive decomposition of flow stress to thermal and athermal components.

In Sec. 2, the role of dislocation dynamics inside the crystal lattice in determining the general form of the thermal plastic stress is investigated using the well-known Orowans' [47] relation that considers the plastic deformation as a dynamic process obtained by the motion of dislocations with an average velocity. In turn, the plastic shear strain rate at the microscale is related to the plastic strain rate tensor at the macroscale using the expression postulated by Bamman and Aifantis [6]. Moreover, the evolution of dislocation density with plastic strain given by Klepaczko [25] is also utilized in the derivation process of the proposed modeling.

In Sec. 3, a constitutive description is presented in order to understand the plastic deformation behavior of bcc, fcc and hcp metals considering the experimental observations as well as the physical basis of the microsturctures inside the material. Both the thermal and athermal components of the flow stress are physically derived and all the models parameters are related to the nano and micro-structure quantities. The hardening stresses are characterized using two different definitions of hardening parameters for each metal structure. Finally, the dynamic strain aging and the twinning phenomena encountered in some polycrystalline metals at certain range of strain rates and temperatures are briefly discussed.

In Sec. 4, the determination procedure of the proposed bcc, fcc and hcp models parameters is presented. Applications of the proposed models to niobium, vanadium, and tantalum for bcc metals, OFHC copper for fcc metals and titanium for hcp are then performed and compared to available experimental results at low and high strain rates and temperatures. Furthermore, discussions

of the model prediction results along with quantification of the nano and micro-quantities are presented. Conclusions are then given in Sec. 5.

2. Dislocation dynamics in crystals under plastic deformation

The plastic behavior of metals can be determined by investigating the dislocation dynamics of their crystals, which are generated, moved and stored during the inelastic deformation. In turn, the most important features that should serve as constituent elements of an appropriate theory of crystal plasticity are the motion, multiplication and interaction of these dislocations. OROWAN [47] recognized the plastic deformation as a dynamic process by suggesting that the plastic shear strain rate is obtained by the motion of dislocations with an average velocity v such that:

$$\dot{\gamma}^p = b\rho_m v, \tag{2.1}$$

where ρ_m is the mobile dislocation density and b is the Burgers vector.

A theoretical description of plasticity should aim at relating the macroscopic deformation behavior at both the intrinsic properties of the deforming material and the externally imposed deformation conditions. On the microscopic scale, the plastic flow of crystalline materials is controlled by the generation, motion and interactions between dislocations. Thus, the constitutive description must, in principle, bridge the entire hierarchy of length scales, starting from the determination of the single dislocation properties on an atomistic scale and proceeding up to the characterization of the macroscopic material properties. In many cases, conclusions about the macroscopic deformation behavior can be obtained by investigating the temperature and strain rate dependence of the flow stress of pure bcc and fcc metals considering the properties of single dislocations (ZAISER *et al.* [58]). In relating the plastic shear strain rate at the microscale to the plastic strain rate tensor at the macroscale, the following expression is postulated (BAMMAN and AIFANTIS, [6]):

$$\dot{\varepsilon}_{ij}^p = \gamma^p M_{ij}, \tag{2.2}$$

where M_{ij} is the symmetric Schmidt orientation tensor which is defined as follows:

$$M_{ij} = \frac{1}{2}(n_i \otimes \nu_j + \nu_i \otimes n_j), \tag{2.3}$$

where $\hat{n}$ denotes the unit normal on the slip plane and $\hat{\nu}$ denotes the unit vector in the slip direction. Equation (2.2) indicates that the climb processes were neglected and plastic incompressibility was assumed since the orientation tensor $\dot{M}_{ij}$ is traceless. Moreover, the variation of the Schmidt tensor is ignored

either by considering that plasticity at the macroscale incorporates a number of differently oriented grains into each continuum point and therefore an average value is assumed or by being the product of two "first order" terms (Aifantis [2] Bammann and Aifantis [7]).

Substituting Eq. (2.1) into Eq. (2.2), the equivalent plastic strain rate $\dot{\varepsilon}_p$ at the macroscale is defined in terms of the mobile dislocation density and dislocation velocity as follows:

$$(2.4) \qquad \dot{\varepsilon}_p = \sqrt{\frac{2}{3}\,\dot{\varepsilon}_{ij}^p \dot{\varepsilon}_{ij}^p} = \bar{m}b\,\rho_m v$$

where $\bar{m} = (2M_{ij}M_{ij}/3)^{1/2}$ can be interpreted as the Schmidt orientation factor. It should be noted that both the mobility v and the concentration ρ_m of dislocations increase with increasing external forces (stresses). Nadgornyi [39] showed that one can (and often should) use the dislocation rate as well as the dislocation velocity interchangeably if one considers plastic deformation quantitatively. Consequently, the meaning of the quantities defined in Eq. (2.1) should be subject to refinement. Voyiadjis and Abed [55] utilized this concept in the derivation of their constitutive models for both bcc and fcc metals. For the present work, however, only the dislocation velocity is considered and rather than incorporating the dislocation rate $(d\rho/dt)$, we consider the variation of the mobile dislocation density with the plastic strain $(d\rho/d\varepsilon_p)$. Therefore, the accumulation of dislocation density from its initial values until reaching its saturated level is considered.

The accumulation process of material dislocation density during the plastic deformation was investigated extensively by many authors (see for example, Klepaczko [25], Kubin and Estrin [31], Bammann [8] and Barlat et al. [9]. Klepaczko [25] showed that the growth of dislocation density is nearly linear with regard to the deformation in the first steps of the hardening process, independently of the temperature. This is followed by a recombination of the dislocations that is assumed to be proportional with the probability of dislocation meeting, that is to say of the dislocation density. Based on this hypothesis, the following simple relation for the evolution of the total dislocation density ρ was presented (Klepaczko, [25]):

$$(2.5) \qquad \frac{d\rho}{d\varepsilon_p} = M - k_a(\rho - \rho_i),$$

where $M = 1/bl$ is the multiplication factor, l is the dislocation mean free path, ρ_i is the initial dislocation density encountered in the material due to the manufacture process or by nature, and k_a is the dislocation annihilation factor which may depend on both the temperature and strain rate. Klepaczko and Rezaig [27]

showed that for mild steels, both M and k_a could be assumed constant at not so high strain rates and up to the temperature where the annihilation micromechanisms (recovery) start to be more intense. It should be kept in mind however, that at saturation, the slope $d\rho/d\varepsilon_p$ approaches the value of zero, which leads to the following definition of the saturated dislocation density ρ_s

$$(2.6) \qquad \rho_s = \rho_i + \frac{M}{k_a}.$$

The mobile dislocation density is related to the total dislocation density ρ by the linear relation ($\rho_m = f\rho$), where the fraction $f \leq 1.0$ may change with ρ and temperature (Kelly and Gillis [24] Sackett et al. [49]). In fact, it can be shown that the constant value of the fraction f gives satisfactory quantitative results for most metals (Klepaczko and Rezaig [27]). In this study, the fraction f represents only the part of the mobile dislocation density that is thermally affected through Orowan's equation as will be discussed later.

Kubin and Estrin [31] proposed the following set of two coupled differential equations to describe both the forest ρ_f and mobile ρ_m dislocation density evolutions with plastic strain using the same above-mentioned concepts:

$$(2.7) \qquad \begin{aligned} \frac{d\rho_m}{d\varepsilon_p} &= \frac{\lambda_1}{b^2} - \lambda_2\rho_m - \frac{\lambda_3}{b}\rho_f^{1/2}, \\[2mm] \frac{d\rho_f}{d\varepsilon_p} &= \lambda_2\rho_m + \frac{\lambda_3}{b}\rho_f^{1/2} - \lambda_4\rho_f, \end{aligned}$$

where the constant coefficients λ_i are related to the multiplication of mobile dislocations (λ_1), their mutual annihilation and trapping (λ_2), their immobilization through interaction with forest dislocations (λ_3), and to the dynamic recovery (λ_4).

The dislocations are assumed to move in a periodic potential and the average dislocation velocity v is determined by the thermodynamic probability of achieving sufficient energy temperature T to move past a peak in the potential. In other words, it is determined through thermal activation by overcoming local obstacles to dislocation motion. Many expressions defining the dislocation speed for thermally activated dislocation glides may be found in the literature (Stein and Low [50] Gillis and Gilman [19], Li [34] and Hirth and Nix [17]). The following general expression, however, is postulated (Bammann and Aifantis [6]):

$$(2.8) \qquad v = v_o \exp\left(-\frac{G}{kT}\right),$$

where k is the Boltzmann's constant, and T is the absolute temperature. The reference dislocation velocity v_o represents the peak value where the temperature reaches or exceeds the melting point. It is defined by $v_o = d/t_w$, where t_w

represents the time that a dislocation waits at an obstacle and d is the average distance the dislocation moves between the obstacles. The shear stress-dependent free energy of activation G may depend not only on stress but also on the internal structure. Kocks *et al.* [28] suggested the following definition to relate the activation energy G to the thermal flow stress σ_{th}:

$$(2.9) \qquad G = G_o \left(1 - \left(\frac{\sigma_{th}}{\hat{\sigma}} \right)^p \right)^q ,$$

where G_o is the reference Gibbs energy, $\hat{\sigma}$ is the threshold stress at which the dislocations can overcome the barriers without the assistance of thermal activation ($\sigma_{th} = \hat{\sigma}$ where $G = 0.0$), and p and q are constants defining the shape of the short-range barriers. According to Kocks [29] the typical values of the constant q are $3/2$ and 2 that is equivalent to a triangular obstacle profile near the top. On the other hand, the typical values of the constant p are $1/2$ and $2/3$ which characterizes the tail of the obstacle.

Substituting Eq. (2.5) for the dislocation density evolution (after performing proper integration) and Eq. (2.8) for the dislocation velocity into Eq. (2.4) and making use of Eq. (2.9), the general relation of the thermal flow stress for polycrystalline materials (metals) is defined as follows:

$$(2.10) \qquad \sigma_{th} = \hat{\sigma} \left[1 - \left(\beta_1(\varepsilon_p)T - \beta_2 T \ln \frac{\dot{\varepsilon}_p}{\dot{\varepsilon}_{po}^i} \right)^{1/q} \right]^{1/p} ,$$

where $\dot{\varepsilon}_{po}^i$ represents the reference equivalent plastic strain rate in its initial stage while related to the initial mobile dislocation. Its order of magnitude can, however, be anywhere between 10^6 and 10^9 s^{-1} which characterizes the highest rate value a material may reach as related to the reference (highest) dislocation velocity v_o,

$$(2.11) \qquad \dot{\varepsilon}_{po}^i = \bar{m} b \, v_o \, \rho_{mi} .$$

The parameters β_1 and β_2 are defined as follows:

$$(2.12) \qquad \beta_1 = \frac{k}{G_o} \ln \left(1 + C_1 \left(1 - \exp(-k_a \varepsilon_p) \right) \right)$$

and

$$(2.13) \qquad \beta_2 = \frac{k}{G_o}$$

where

$$(2.14) \qquad C_1 = f \frac{M}{k_a \rho_{mi}} .$$

It is worthwhile to mention here that β_1 is not constant and rather increases with plastic strain increase. Its value, however, attains the maximum when the mobile part of the total dislocation density reaches its saturated level ($\rho_m = \rho_{ms}$), which is the case at high strains. On the other hand, β_1 vanishes as the plastic strain approaches zero and, in consequence, the thermal plastic flow pertains totally to the yield stress. In this work, the fraction f, which represents the mobile portion amount of the total dislocation density, is assumed constant in order to simplify the determination procedure of the model parameters. Moreover, average values of the quantities M and k_a are considered (KUBIN and ESTRIN, [31]).

In understanding quantitatively the deformation behavior of metals, a constitutive description is required. In fact, any constitutive modeling of crystalline materials like metals should consider the physical basis of the microstructure inside the material as well as the experimental observation during the plastic deformation. However, deforming a metal beyond its elastic limit activates and moves its dislocations through the crystal. In turn, two types of obstacles are encountered that try to prevent dislocation movements through the lattice; short-range and long-range barriers. The short-range ones are due to dislocations trapping (forest) which can be overcome by introducing thermal energy through the crystal. On the other hand, the long-range barriers are due to the structure of the material, which cannot be overcome by introducing thermal energy through the crystal. Therefore, the flow stress of any type of metals ($\sigma = (3\sigma_{ij}\sigma_{ij}/2)^{1/2}$ of the von Mises type) will be additively decomposed into two major components; the athermal stress σ_a and the thermal stress σ_{th}

$$(2.15) \qquad\qquad\qquad \sigma = \sigma_{th} + \sigma_a.$$

The above assumption of additive decomposition for the formulation of the flow stress has been proved experimentally and is used by several authors (see for example, ZERILLI and ARMSTRONG [59], NEMAT-NASSER and ISAACS [41] and NEMAT-NASSER et al. [43]).

Although Eq. (2.10) represents the general relation of the thermal stress, the final definition of thermal stress as well as athermal stress differs from metal to metal, depending, on both the microstructure crystal shape (bcc, fcc, and hcp) and on the experimental observations. In the following section, constitutive relations will be proposed for different types of metals applicable to high strain rates and temperatures.

3. Constitutive modeling of polycrystalline metals

Based on their crystal structure, metals can generally be classified into three major types; body-centered cubic (bcc), face-centered cubic (fcc), and hexagonal

close-packed (hcp). The crystal structure and the atom distribution inside the lattice play a crucial role in controlling the dislocation generation and movement during plastic deformation. Each type of metal, however, has its own behavior coupled to strain rate and temperature. In this section, modeling of the plastic flow is presented for the aforementioned types of metals using the thermal activation energy principle combined with systematic experimental observations investigated by many authors. On the other hand, the role of solute/dislocation interaction in metals is not included in this study and therefore, the temperatures and strain rates are considered in the range where dynamic strain aging (DSA) is not effective.

3.1. Body centered cubic (BCC) metals

Experimental observations of most bcc metals, such as pure iron, tantalum, niobium and vanadium show strong dependence of the yield stress on the strain rate and temperature, whereas the plastic hardening is hardly influenced by temperature. That is, at a given strain rate and different temperatures or at a given temperature and several strain rates, the variation of the stress-strain curves appear only on the yielding point whereas the hardening curves are almost identical (e.g. see Fig. 1 for the case of vanadium). This indicates that the thermal component of the flow stress is mainly controlled by the yield stress and nearly independent of the plastic strain.
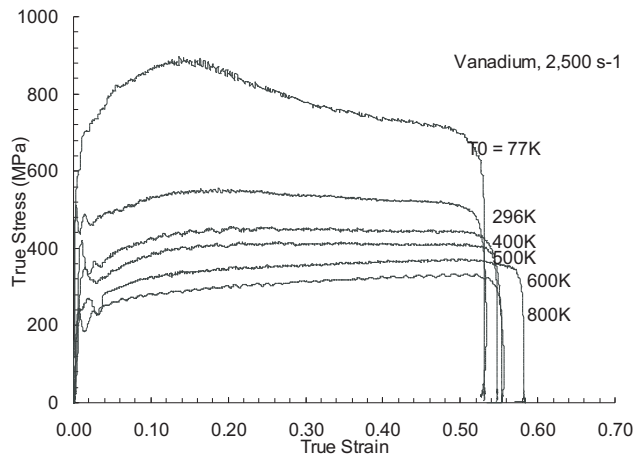
FIG. 1. Adiabatic flow stress of vanadium for indicated initial temperatures, at 2500 s^{-1} strain rate given by NEMAT-NASSER and GUO [44, 45].

The thermal stress of bcc metals may be interpreted physically as the resistance of the dislocation motion by the Peierls barriers (short-range barriers) provided by the lattice itself. Moreover, the thermal component of the flow stress for

such metals can be determined using the same expression defined in Eq. (2.10). In fact, it is found for most bcc metals that the effect of the variation of β_1 (or variation of mobile dislocation density) on the thermal flow stress is practically negligible as will be shown in the application section. This behavior, actually, comes out from the fact that the plastic hardening is essentially allotted to the athermal part of the flow stress which is primarily accomplished through the relatively temperature-insensitive long-range barriers.

It should be mentioned here that the flow stress at a given temperature, T, is proportional to an appropriate shear modulus, μ, at this temperature. It is also necessary to have G proportional to $\mu(G \propto \mu b^3)$ in order for the activation work done by the applied forces during the activation event to be independent of material properties (KOCKS [29]). ZERILLI and ARMSTRONG [59] related, at zero Kelvin temperature, the thermal stress (σ_o) to the reference Gibbs energy (G_o) and dislocation activation area (A_o) as follows:

$$(3.1) \qquad \sigma_o = \frac{mG_o}{A_o b},$$

where b is the magnitude of the Burgers vector and m is the orientation factor that relates the shear stress to the normal stress, $\sigma = m\tau$ where $m = \sqrt{3}$ for the case of the von Mises flow rule. Utilizing Eq. (3.1) with a proper proportional relation of the reference Gibbs energy to the shear modulus, the parameter $\hat{\sigma}$ can be related to the strain-independent internal structure as follows:

$$(3.2) \qquad \hat{\sigma} = m\alpha_o\mu_o b^2/A_o,$$

where α_o is a constant which represents the portion of the shear modulus μ_o contributed to the activation energy, both at zero temperature. For bcc metals, the activation area A_o may be considered to be constant in accordance with the intrinsic Peierls stress.

For most metals, an additional component of stress Y_a is used that is independent of plastic strain and temperature (athermal yield stress component) and related to the internal microstructure quantities that are independent of plastic strain (e.g. grain diameter D_g). This component is defined as the product of microstructural stress intensity and the inverse square root of the average grain diameter. KLEPACZKO [26] proposed a definition for the stress intensity as related to the shear modulus and the magnitude of the Burgers vector from which the athermal yield stress is finally defined as follows:

$$(3.3) \qquad Y_a = \alpha_1\mu\left(\frac{b}{D_g}\right)^{1/2}$$

where α_1 is the interaction constant showing the contribution of the above mechanism to the athermal stress.

The final component of the bcc flow stress is attributed to the hardening stress, which is independent of temperature, and consequently contributes to the athermal flow stress part. In fact, both the mobile dislocation density and immobile (forest) dislocation density should be considered in the evolution (accumulation) relations for the case of large strain problems (up to 50%). Therefore, the hardening component of the flow stress is related to the effective total dislocation density ($\bar{\rho} = \rho - \rho_i$) where ρ_i is the initial dislocation density encountered originally inside the material. The dislocation model of Taylor [52] gives the shear flow stress τ in terms of the total dislocation density ρ as

$$(3.4) \qquad\qquad \tau = \alpha \mu \, b \sqrt{\rho},$$

where α is an empirical coefficient taken to be 0.2 for fcc metals and about 0.4 for bcc metals as given by Nabarro et al. [38], who pointed out that Eq. (3.4) can be derived by several methods. Ashby [3] split the difference of α values in assuming that $\alpha = 0.3$ for most metals. The plastic strain evolution of the effective total dislocation density can be defined, after solving the differential equation Eq. (2.5), in terms of the internal physical quantities as follows:

$$(3.5) \qquad\qquad \bar{\rho} = \frac{M}{k_a} \left(1 - \exp(-k_a \varepsilon_p)\right).$$

Relating the shear stress to the normal stress by $\sigma = m\tau$, and substituting $\bar{\rho}$ defined by Eq. (3.5) instead of ρ in Eq. (3.4), one has the athermal flow stress in the following form:

$$(3.6) \qquad\qquad \sigma_a = Y_a + \bar{B}(1 - \exp(-k_a \varepsilon_p))^{1/2},$$

where $\bar{B}$ is the hardening parameter defined as

$$(3.7) \qquad\qquad \bar{B} = m\alpha\mu b \left(M/k_a\right)^{1/2}.$$

Alternatively, the plastic hardening for pure bcc metals may be evaluated from an assumed power law dependent on strain. This assumption is observed experimentally and used by many authors (see for example Zerilli and Armstrong [59] and Nemat-Nasser et al. [43]). Thus, the athermal flow stress of bcc metals may be given as

$$(3.8) \qquad\qquad \sigma_a = Y_a + B\varepsilon_p^n$$

where B and n are the hardening parameters. This experimental observation can be physically justified by using alternative explanation for the total dislocation density. In other words, the total dislocation density may also be defined as the

interaction between the density ρ_s for statistically stored dislocations, which are stored by trapping each other in a random way, and density ρ_g for geometrically necessary dislocations, which are stored in order to maintain the continuity (compatibility) of various components of the material, i.e.

$$(3.9) \qquad \rho^\gamma = \rho_s^\gamma + \rho_g^\gamma,$$

where the exponent γ is a material parameter. ASHBY [3] pointed out that, in general, the presence of geometrically necessary dislocations will accelerate the rate of statistical storage and that the value of $\gamma = 1$ should provide a lower limit on the effective total dislocation density. Based on that, ZHAO *et al.* [61] argued that the value of γ should be less than or equal to 1 in order to properly estimate the effective total dislocation density.

It is obvious from the above definitions of both dislocation densities that the geometrically necessary dislocation density ρ_g is related to the strain gradient whereas the statistically stored dislocation density ρ_s is related to the strain hardening as follows (ZHAO *et al.* [61]:

$$(3.10) \qquad \rho_g = \hat{f}\frac{\chi}{b}, \qquad \rho_s = \left(\frac{\sigma_{\text{ref}}\varepsilon^N}{m\alpha\mu b}\right)$$

where χ is a suitable form of the third-order strain gradient tensor and $\hat{f}$ is a function of higher order gradients of strain. The function $\hat{f}$, however, becomes constant when the strain-gradient field is uniform. The coefficients σ_{ref} and N represent the material parameters for the assumed power-law hardening rule. Eq. (3.10) may be used for the definition of both the effective statistically stored dislocation density $\bar{\rho}_s$ and the effective geometrically necessary dislocation density $\bar{\rho}_g$ except that they are related to the plastic strain and the plastic strain gradient respectively.

By substituting Eq. (3.10) into Eq. (3.9), the power-law hardening parameters can be related to the effective statistically stored dislocation density $\bar{\rho}_s$ for the case of uniform plastic straining ($\bar{\rho}_g \simeq 0$) as follows:

$$(3.11) \qquad \sigma_{\text{ref}}\varepsilon_p^N = m\alpha\mu b\sqrt{\bar{\rho}_s}.$$

Although the above equation (Eq. (3.11)) rationalizes the power-law hardening rule by relating it to the internal physical quantities, the hardening parameters B and n, however, are not explicitly defined as in the case of those given by Eq. (3.6). In turn, the athermal hardening stress may be estimated either by using the physically derived relation given by Eq. (3.6) or by using the empirical relation, Eq. (3.8), obtained through experimental observations.

Accordingly, the total flow stress for bcc metals may be calculated, after making use of the concept of additive decomposition in Eq. (2.15), through one of the following relations:

$$(3.12) \qquad \sigma = Y_a + \bar{B}\left(1 - \exp(-k_a \varepsilon_p)\right)^{1/2}$$

$$+ \hat{\sigma}\left[1 - \left(\beta_1(\varepsilon_p)T - \beta_2 T \ln \frac{\dot{\varepsilon}_p}{\dot{\varepsilon}_{po}^i}\right)^{1/q}\right]^{1/p}$$

and

$$(3.13) \qquad \sigma = Y_a + B\varepsilon_p^n + \hat{\sigma}\left[1 - \left(\beta_1(\varepsilon_p)T - \beta_2 T \ln \frac{\dot{\varepsilon}_p}{\dot{\varepsilon}_{po}^i}\right)^{1/q}\right]^{1/p}$$

The above relations may be used to predict the stress-strain curves for both isothermal and adiabatic plastic deformations. For the case of isothermal deformation, the temperature T remains constant during the plastic (representing the initial testing temperature, T_o) deformation. In the adiabatic case of deformation, heat inside the material increases as plastic strain increases and therefore, the temperature T is calculated incrementally by assuming that the majority of the plastic work is converted to heat:

$$(3.14) \qquad T = T_o + \frac{\zeta}{c_p \rho} \int_0^{\varepsilon_p} \sigma d\varepsilon_p.$$

Here ρ is the material density and c_p is the specific heat at constant pressure. The Taylor–Quinney empirical constant ζ is often assigned the value of 0.9. However, recent tests have indicated that this parameter may vary with plastic strain (for more details see the work of Kapoor and Nemat-Nasser, [23]). Equation (3.14) may be solved numerically or can be integrated without introducing any noticeable errors by either using the mean value theorem or the simple Euler method. In this work, Eq. (3.14) is used for all types of metals to determine the evolution of temperature with plastic strain throughout the adiabatic deformation.

It should be noted that the thermal component of the flow stress given by the last term in the right-hand side of Eq. (3.12) or Eq. (3.13) is non-negative. Thus, the term between the brackets on the right-hand side should be set equal to zero when the temperature exceeds the critical value. The critical temperature, in the T vs σ curve, defines the starting point of the constant stress which represents the athermal component of the flow stress. This critical value, however, is strain rate dependent and is defined as follows:

(3.15)
$$T_{\text{cr}} = \left(\beta_1 - \beta_2 \ln \frac{\dot{\varepsilon}_p}{\dot{\varepsilon}_{po}^i} \right)^{-1}.$$

3.2. Face centered cubic (FCC) metals

In the case of fcc metals, like copper and aluminum, the mechanisms of thermal activation analysis are dominated and controlled by the emergence and evolution of a heterogeneous microstructure of dislocations (mobile) as well as the long-range interactions between dislocations (forest). On this basis, the thermal activation is strongly dependent on the plastic strain. That is, the increase in the yield point with a decrease in temperature is highly dependent on the strain-hardened states for fcc metals. Experimental observations validate the plastic strain dependence of strain rate and temperature for most fcc metals (NEMAT-NASSER and LI [40], TANNER et al. [51], LENNON and RAMESH [33]). That is, for a certain strain rate and various temperatures, the adiabatic stress vs strain plots clearly show that all curves start approximately from the same point (initial yielding) and each curve hardens differently from each other, depending on the corresponding temperature (see Fig. 2 for the case of OFHC Copper).
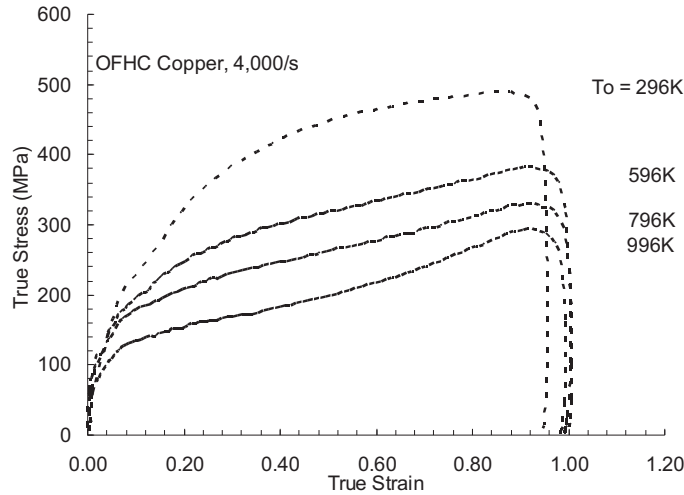
FIG. 2. Adiabatic flow stress of OFHC copper for indicated initial temperatures, at 4000 s^{-1} strain rate given by NEMAT-NASSER and LI [42].

The effect of mobile dislocation density is introduced to the flow stress by utilizing Orowan's equation as derived in the previous section. That is to say, the parameter β_1 plays a significant role in characterizing the effect of dislocations movement on the thermal flow stress during the thermal plastic deformation. Additionally, for the thermal activation analysis behavior, the effect of dislocation

intersection mechanisms (mobile and forest) on the flow stress can be described as follows. When dislocation patterns (i.e. cell) are formed, the sources of mobile dislocations become numerous in the cell walls. After deformation, dislocations tend to be trapped on the next cell wall forming a forest of dislocations, which become the major obstacle for a mobile dislocation. Therefore, introducing thermal energy will facilitate dislocations in overcoming these types of obstacles and, in consequence, provide hardening to the thermal flow stress.

On this basis, the distance d between dislocation intersections and consequently the activation volume play an additional crucial role in determining an appropriate formulation introducing the effect of plastic strain on the thermal component of the material flow stress. Thus, the activation volume V can be related to the distance between dislocation intersections as follows (ZERILLI and ARMSTRONG [59], VOYIADJIS and ABED [55]):

$$(3.16) \qquad\qquad V = Ab = db^2/2,$$

where A is the activation area. In fact, GRACIO [20] has speculated that in copper, when the plastic strain increases, the mean free path decreases and consequently, the distance between dislocation intersections decreases. Therefore, the forest dislocation densities as well as the plastic strain are related to the distance d through the relationship (KUBIN and ESTRIN [31])

$$(3.17) \qquad\qquad d \sim 1/\varepsilon_p^{1/2} \qquad \text{and} \qquad \rho_f \sim 1/d^2.$$

The multiple slip-crystal flow stress for fcc metals at $T = 0.0$ Kelvin temperature and any strain value is related to both the dislocation densities and strain by the relation given by several authors (see for example BELL [11])

$$(3.18) \qquad\qquad \sigma_o \simeq \sigma_o'(b/d) \simeq \sigma_o''\varepsilon_p^n.$$

Comparing Eq. (3.18) with Eq. (2.10) for the case of zero Kelvin temperature, and employing the argument given by Eqs. (3.16) and (3.17), the activation area A_o for fcc metals, determined by dislocation intersections, is proportional to the inverse square root of plastic strain (and vice versa) as follows (ZERILLI and ARMSTRONG [59]):

$$A_o = A_o' \varepsilon_p^{-1/2}$$

$$(3.19) \qquad\qquad \text{or}$$

$$A_o^{-1} = A_o'^{-1}\varepsilon_p^{1/2}$$

Equation (3.19) clearly shows that the activation area decreases as the plastic strain evolves which indicates that the value of the activation area is the highest

at the initial stage of plastic deformation ($\varepsilon_p = 0$). The initial activation area, however, is a finite quantity, which is not the case as defined in Eq. (3.19) since it will tend to infinity when the plastic strain is zero. In this work, therefore, the definition of the initial activation area is modified by incorporating a finite initial activation area A_o', and defined for the case of fcc metals as follows:

$$(3.20) \qquad A_o^{-1} = A_o'^{-1} + A_o''^{-1}\varepsilon_p^{1/2}.$$

Substituting Eq. (3.20) into Eq. (3.1) and since $\sigma_o = \hat{\sigma}$ at $T = 0$, the thermal component of the present constitutive equation for the case of fcc metals will incorporate the coupling of temperature, strain rate, as well as plastic strain. On the other hand, the athermal component of fcc flow stress is independent of the plastic strain and it pertains totally to the initial yield stress and is related to the internal structure (grain diameter) as in the case of bcc metals Eq. (3.3). Using the additive decomposition given in Eq. (2.15), the total flow stress may then be defined for the case of fcc metals as:

$$(3.21) \qquad \sigma = Y_a + \left(\tilde{B}\varepsilon_p^{1/2} + Y_d\right)\left[1 - \left(\beta_1(\varepsilon_p)T - \beta_2 T\ln\frac{\dot{\varepsilon}_p}{\dot{\varepsilon}_{po}^i}\right)^{1/q}\right]^{1/p},$$

where the parameters Y_a and β_i are the same as defined previously, whereas the hardening parameter $\tilde{B}$ is given as:

$$(3.22) \qquad \tilde{B} = m\alpha_o\mu_o b^2/A_o''.$$

It can be seen in Eq. (3.21) that, at a given plastic strain value, the thermal stress preserves the same trend shown in bcc metals including that constants p and q are falling in the same range as those given before. Moreover, there is no strain rate and temperature effect on the initial yield stress and, thus, Y_a is constant.

In fact, the modification of the activation energy definition given in Eq. (3.20) guided us in introducing an additional component to the thermal flow stress, incorporating the electron- and phonon- drag effects on the movement of material dislocations. This phenomenon is encountered mainly in fcc and hcp metals at the regions where the plastic strains approach zero with relatively high strain rates (JASSBY and VREELAND [21] and ZERILLI and ARMSTRONG [60]). An examination of Eq. (3.21) shows that when the plastic strain approaches the limit zero ($\varepsilon_p \to 0.0$), the solution for the thermal stress approaches the limiting value

$$(3.23) \qquad \sigma_{th} \to Y_d\left[1 - \left(\frac{k}{G_o}T\ln\frac{\dot{\varepsilon}_{po}^i}{\dot{\varepsilon}_p}\right)^{1/q}\right]^{1/p},$$

where the parameter Y_d may be considered as the resultant drag-stress at the reference velocity $\dot{\varepsilon} = \dot{\varepsilon}_o$ and/or zero Kelvin temperature $T = 0$ defined as

$$(3.24) \qquad Y_d = m\alpha_o\mu_o b^2 / A_o'.$$

It's obvious that the drag-stress component given by Eq. (3.23) is a decreasing function of temperature whereas it increases with the increase of the strain rate. Such a behavior, however, coincides with the experimental results and observations found in the literature (see Vreeland and Jassby [56] and Follansbee et al. [15], Nemat-Nasser and Li [40] and Nemat-Nasser et al. [46]). In this regard, Armstrong et al. [5] have noted that the strong upturn in flow stress at high strain rates signifies a strong decrease in the activation area A, approaching atomic dimensions, indicative of strongly reduced intersection spacing leading to the dislocation density increase.

Actually, the hardening parameter $\tilde{B}\varepsilon_p^n$ given in Eq. (3.21) can alternatively be derived by a more accurate method by relating the activation area to the forest dislocation density after utilizing both Eqs. (3.16) and (3.17) as follows:

$$(3.25) \qquad A_o = bd/2 \simeq \tilde{m}b\rho_f^{-1/2},$$

where $\tilde{m}$ is a constant and the evolution of forest dislocation density with plastic hardening may be defined after making use of Eq. (2.5) as follows:

$$(3.26) \qquad \rho_f = \rho_{fi} + \bar{f}\frac{M}{k_a}\left(1 - \exp(-k_a\varepsilon_p)\right),$$

where $\bar{f}$ denotes the forest dislocation density fraction of the total dislocation density. Substituting Eq. (3.25) into Eq. (3.2) and utilizing Eq. (3.26), the plastic flow stress of fcc metals can alternatively be determined using the following relation:

$$(3.27) \qquad \sigma = Y_a + \left(\hat{Y}_d + \hat{B}\left(1 - \exp(-k_a\varepsilon_p)\right)^{1/2}\right),$$

$$\times \left[1 - \left(\beta_1(\varepsilon_p)T - \beta_2 T \ln \frac{\dot{\varepsilon}_p}{\dot{\varepsilon}_{po}^i}\right)^{1/q}\right]^{1/p},$$

where the hardening parameter $\hat{B}$ and the drag-stress component $\hat{Y}_d$ are defined by the following two relations:

$$(3.28) \qquad \hat{B} = \hat{m}\alpha_o\mu_o b\sqrt{\bar{f}\frac{M}{k_a}},$$

$$(3.29) \qquad \hat{Y}_d = \hat{m}\alpha_o\mu_o b\sqrt{\rho_{fi}},$$

where $\hat{m} = m/\tilde{m}$ is a constant. The plastic flow stress for bcc metals is then determined using either Eq. (3.21) with a power low hardening stress component or Eq. (3.27) with a more accurate physical interpretation of hardening stress. Both relations, however, correlate properly with the experimental results.

As a final point, the evolution of the adiabatic temperature for fcc metals is simulated using the same evolution relation given in Eq. (3.14). Moreover, the critical temperature of fcc metals is both strain and strain rate-dependent and is defined in the same way as that given in Eq. (3.15).

3.3. Hexagonal Close-Packed (HCP) Metals

The mechanical behavior of hcp metals, like titanium and zirconium, can be determined by addressing the structure and energies of dislocation cores and planer defects, including twin boundaries and stacking faults. However, different hcp materials have dramatically different mechanical properties which make the modeling of the plastic flow of hcp metals very complicated and not unique over broad temperature and strain rate ranges. In fact, hcp materials often show strong temperature-dependent behavior, often associated with changes in deformation modes which, in turn, affect both the polycrystalline ductility and dynamic recrystallization. Although the crystal structure of hcp metals is close-packed like fcc metals, it shows plastic anisotropy and lacks the symmetry needed to be sufficient in satisfying, for instance, the von Mises criterion (YOO et al. [57]). Since each hcp metal has its own mechanical behavior depending on the internal structure (a/c ratio) and slip plane and direction, the authors choose to concentrate in this study only on the thermal plastic deformation behavior of titanium. Its alloys are considered to be the most increasingly used hcp metals in structural applications at low and high strain rate of loading.

Observations of the experimental stress-strain results of titanium under high strain rates and elevated temperatures indicated that not only is the yield stress strongly dependent on temperature and strain rates but the strain hardening also changes with temperatures, as shown in Fig. 3.

Figure 3 implies that thermal activation has the effect of both lowering the yield stress and decreasing the effect of strain hardening. Thus, the macroscopic thermomechanical behavior of hcp metals in general and titanium in particular, tends to fall somewhere between that of the fcc and bcc metals. In this regard, the plastic flow stress of hcp metals is related to temperature and strain rates assuming that the plastic flow is mainly accounted for by dislocation motion and intersections, as follows:

$$(3.30) \quad \sigma = Y_a + B\varepsilon_p^n + \left(\tilde{B}\varepsilon_p^{1/2} + Y_d \right) \left[1 - \left(\beta_1(\varepsilon_p)T - \beta_2 T \ln \frac{\dot{\varepsilon}_p}{\dot{\varepsilon}_{po}^i} \right)^{1/q} \right]^{1/p}$$

or

(3.31) $\quad \sigma = Y_a + \bar{B}\left(1 - \exp(-k_a\varepsilon_p)\right)^{1/2}$

$\qquad + \left(\hat{B}\left(1 - \exp(-k_a\varepsilon_p)\right)^{1/2} + Y_d\right)\left[1 - \left(\beta_1(\varepsilon_p)T - \beta_2 T\ln\frac{\dot{\varepsilon}_p}{\dot{\varepsilon}_{po}^i}\right)^{1/q}\right]^{1/p}.$
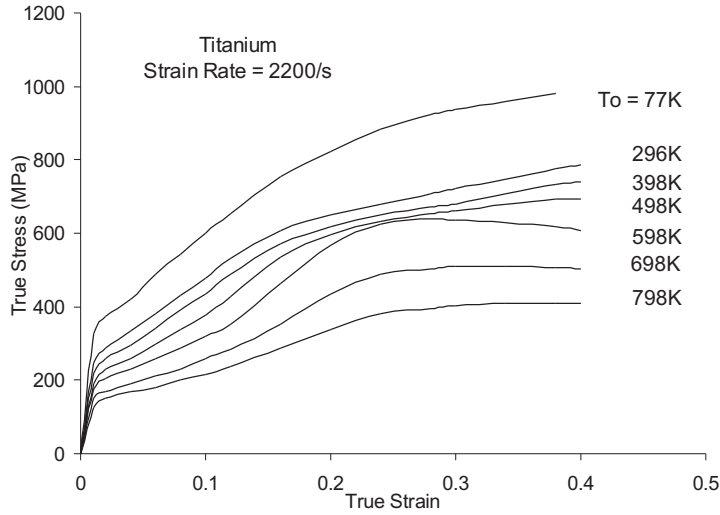
FIG. 3. Adiabatic flow stress of titanium for indicated initial temperatures, at 2200 s^{-1} strain rate given by NEMAT-NASSER *et al.* [43].

The first two terms in Eq. (3.30) and Eq. (3.31) represent the athermal part of the flow stress whereas the third term represents the thermal coupling of plastic hardening and yield stress to the flow stress.

Recent research by CHICHILI *et al.* [13] on α-Ti indicated that twin-dislocation intersections play an important role in strain hardening at room temperature and for strain rates ranging from 10^{-5} to 10^2 s^{-1}. In contrast, the experimental study of NEMAT-NASSER *et al.* [43] for the plastic flow of commercially pure titanium at strain rates from 10^{-3} to 10^3 s^{-1} and temperatures from 77 to 1000 K, with strains exceeding 40%, showed that the high density of twins does not necessarily correlate with a higher flow stress. On the other hand, they illustrated that the dynamic strain aging takes place at both low and high strain rates and for a wide range of temperatures. Accordingly, any constitutive relation that deals with the thermomechanical response of titanium should consider not only the role of dislocation activities (dislocation motion and intersections) but also the role of dynamic strain aging as a major event with the role of deformation twinning being uncertain.

In this study, nevertheless, the plastic flow relation defined in Eq. (3.30) is limited to temperature and strain ranges where both twinning and dynamic strain aging is not activated. A brief description of twinning and DSA behaviors is presented in the following sections. The effect of dynamic strain aging on the flow stress of metals, however, is of considerable current interest to the authors and an extensive study of this phenomenon is going to be presented in a forthcoming paper.

3.3.1. Dynamic strain aging (DSA).

The dynamic strain aging can be interpreted physically as the diffusion of solutes atoms to the mobile dislocations that are temporarily trapped at an obstacle for a certain amount of time before they jump to another obstacle. The activation of DSA takes place when the aging time is equal to the waiting time of these dislocations and therefore, the obstacle strength is increased by certain amount. Dynamic strain aging may be observed at different strain rate levels and certain range of temperatures. It may occur either through a directional diffusion of the dislocation core atmosphere, at high strain rates, or through a bulk diffusion, at low strain rates (NEMAT-NASSER et al. [43]).

The dynamic strain aging behavior can be described macroscopically as the sudden increase of the flow stress at certain temperature that normally causes a decrease in the flow stress curve. In other words, at fixed strain and strain rate, and with temperature increase, the decreasing flow stress may suddenly begin to increase at a certain temperature and, after attaining a peak value, may begin to decrease. This sudden increase and decrease of stress forms a noticeable hump in the flow stress-temperature curve. The peak value of the flow stress, however, changes with strain and strain rates. Moreover, the temperature value which indicates the start of the sudden increase in the flow stress is also strain rate dependent.

The range of temperature and strain rate where the DSA is displayed differs from metal structure to another and even from metal to metal within the same crystal structure. Experimental results of Nemat-Nasser and co-workers on bcc and fcc metals (NEMAT-NASSER and ISSACS [41], NEMAT-NASSER and LI [42], NEMAT-NASSER and GUO [44] and CHENG and NEMAT-NASSER [12]) show that Niobium exhibits dynamic strain aging at low strain rates only (around 10^{-3} s^{-1}) for a temperature range of 450–700 K. On the other hand, the DSA behavior is not encountered in tantalum, vanadium and OFHC copper at ranges of 10^{-3} – 10^5 s^{-1} strain rates and 77–1000 K temperatures. For the case of Titanium, the dynamic strain aging is widely encountered at both low and high strain rates and suitable temperature ranges. It is concluded that the DSA behavior is strain rate dependent for all types of metals and it takes place when the deformation temperature approaches its critical value defined in Eq. (3.15).

As addressed by many authors, the thermomechanical modeling of the extra flow stress produced by the effect of dynamic strain aging is not a straightforward procedure. However, as cited by Barlat *et al.* [9], Louat [35] has given a mathematical expression for the extra flow stress σ_D as follows:

$$(3.32) \qquad \sigma_D = \hat{\sigma}_D \left(1 - \exp\left[-(t_w/t_x)^{2/3}\right]\right),$$

where $\hat{\sigma}_D$ is the maximum stress increase produced by the DSA and t_x is the relaxation time associated with diffusion. Equation (3.32) indicates that the extra flow stress vanishes as the waiting time t_w approaches zero. This waiting time can simply be related to the plastic strain by utilizing Orowan's equation, after neglecting the running time of the dislocation between obstacles, as follows

$$(3.33) \qquad t_w = \frac{\bar{m} b d \, \rho_m}{\dot{\varepsilon}_p}.$$

The relaxation time t_x associated with diffusion, on the other hand, is related to the temperature and the microstructure physical parameters as follows (Friedel [16], Kubin and Shihab [32]):

$$(3.34) \qquad t_x = \frac{k T b^2}{3 W D} \left(c_1/\pi c_o\right)^{3/2}.$$

where c_o and c_1 are the bulk solute volume fraction and the saturation solute concentration on dislocations respectively, D is the diffusion coefficient of solute atoms, and W is the absolute value of binding energy between the solute and dislocations. Hence, employing Eqs. (3.32), (3.33) and (3.34) with the DSA being effective at $T \to T_{\mathrm{cr}}$, the additional flow stress could suitably be added in calculating the total flow stress for certain metals.

3.3.2. Deformation twinning behavior. The unusual difficulty associated with identification of deformation mechanisms within hcp metals may be attributed to the fact that these closed-packed crystal structures often exhibit both slip and twinning during plastic deformation. The presence of twin systems, in certain cases, becomes necessary in order to maintain the compatibility of polycrystalline deformation, and it is expected that twinning shear will contribute to the overall strain. This contribution, however, is still inconsistent and uncertain.

Experiments conducted by Nemat-Nasser *et al.* [43] investigated commercially pure titanium over a temperature range of 77–1000 K and strain rates of 10^{-3}–10^4 s^{-1} and showed that deformation twins were observed in most temperatures. Moreover, they illustrated that the density of twins increases with increasing strain rate to 2200 s^{-1}, and when the temperature is decreased to 77 K. Besides, they demonstrated that at 10% true strain and low strain rate, the twins

start disappearing as soon as the temperature exceeds a limiting value of 600K. However, it is shown that the amount of gross deformation produced by twins is relatively small since the relative atomic movement is limited in deformation twinning and hence, most of the plastic flow occurs by the motion of the twins and their intersections. It is concluded, therefore, that though the deformation of the material undergoes high density of twins at high strain and strain rates, it does not correlate with a higher flow stress.

Chichili *et al.* [13], on the other hand, summarized the microstructure characterization of the room temperature deformation of α-titanium as follows: (1) the material deformation at low strain rates and low strains is mainly due to dislocation motion with very few twins; (2) at large strains with the same low strain rate level, it is noted that the increase of the numbers of twins as well as a substantial dislocation motion is observed during the deformation; (3) at high strain rates and small strains, densities of both dislocation motion and twins are obviously increased; (4) by increasing both strains and strain rates, the twin density increases even further, with substantial twin-dislocation interactions. It is concluded, however, that even when the material is heavily twinned, the amount of plastic deformation contributed by twinning is measured to be much less that due to dislocations. Consequently, incorporating such effect in the constitutive modeling of pure titanium is still problematic and inconclusive.

4. Applications, comparisons, and discussions

The proposed constitutive models derived in the previous section for bcc, fcc and hcp metals are further evaluated by direct comparison to the experimental results that are mainly provided by Nemat-Nasser and his co-workers for different types of polycrystalline metals conducted at a wide range of strain rates and temperatures. In this section, the evaluation of the material parameters of the proposed models is first discussed. Applications of these models for predicting the plastic deformation as well as comparisons to experimental results are then illustrated for three bcc metals (niobium, tantalum and vanadium), one fcc metal (OFHC copper) and one hcp metal (titanium) over a wide range of temperatures and strain rates. Finally, numerical identification is also presented for the nano/micro-structural physical quantities used in the definition of the proposed models parameters.

4.1. Model parameters evaluation

Various techniques can be used to determine the material parameters of the proposed models. However, a simple approach is used and similarly applied for all the proposed models with little variation between the three structural types of metals as given by Eq. (3.12) and Eq. (3.13) for bcc metals, Eq. (3.21) and

Eq. (3.27) for fcc metals, and Eq. (3.30) and Eq. (3.31) for hcp metals. The evaluation procedure is initiated by studying the stress-temperature relation at different values of plastic strain and at certain strain rate value. Generally, the flow stress decreases as the temperature increases until a point where the stress is constant with further increase in temperature. These constant values represent the athermal part of the flow stress which varies with plastic strain for the case of bcc and hcp metals, whereas it is strain-independent for the case of fcc metals. Employing the variation of the athermal flow stress with plastic strain, the parameters (B and n or $\bar{B}$ and k_a) for bcc and hcp metals models is calculated using the nonlinear least-squares fit. The Y_a value, on the other hand, represents the athermal stress at zero plastic strain or the athermal component of the initial yield stress. Subtracting the above stress increments (athermal stress) values from the total flow stress, the thermal component of the flow stress is then determined.

The thermal component of the flow stress is mainly pertained to the yield stress for bcc metals and to the plastic hardening for both fcc and hcp metals. Moreover, the thermal degradation mechanism is captured by selecting proper values of the exponents p and q that are chosen here to be $1/2$ for the former and $3/2$ for the latter for all kinds of metals used in this study. Once these exponents are determined for a particular mechanism, they become constants. Next, the intercepts of the constant slope line plotted between σ_{th}^p and $T^{1/q}$ at different plastic strains and certain strain rate are employed here to obtain at zero plastic strain, the threshold stress $\hat{\sigma}$ for bcc models and the parameter Y_d for fcc and hcp models. On the other hand, the hardening parameter $\tilde{B}$ or $\hat{B}$ for fcc and hcp models are determined using the nonlinear least-square fit technique for the different plastic strain intercept values. Then, for the case of bcc models, a graph of $(1 - (\sigma_{th}/\hat{\sigma})^p)^q$ vs $\ln \dot{\varepsilon}_p$ is utilized to determine the parameter β_2 and the reference plastic strain rate $\dot{\varepsilon}_{po}^i$. A similar procedure is followed for the case of fcc and hcp models except that $\hat{\sigma}$ is replaced by Y_d. Finally, the parameter β_1 or the constant C_1 is then determined after detecting all other stress components from the total flow stress at different plastic strain values using the nonlinear least-square fit.

4.2. Applications and comparisons

4.2.1. Bcc metals. Three bcc metals are used in this study as applications for the proposed bcc models: (1) niobium (Nb) is a silvery bcc metal that is used as an alloying agent in carbon and alloy steels, as it improves the strength of the alloy; (2) vanadium (V) is a bright white bcc metal, and is soft and ductile with good structural strength. It is used in the aerospace industry in titanium alloys; (3) tantalum (Ta) has generated a lot of interest in industry due to its density, strength and ductility over a wide range of deformation rates and tem-

peratures. The material parameters of these bcc metals are determined following the procedure discussed previously. The experimental data presented by NEMAT-NASSER and GUO [44, 45] is utilized for the case of Nb and V metals, whereas the parameters of Ta are obtained using the experimental results presented by NEMAT-NASSER and ISAACS [41] and compared also to different results offered by different authors. The numerical values of the material parameters defined by the proposed bcc models are listed in Table 1 for the above-mentioned three metals obtained using the aforementioned procedure.

It is obvious that the only difference between the two proposed bcc models Eq. (3.12) and Eq. (3.13) is with regard to the two different definitions of the plastic hardening component which is mostly associated to the athermal component of the flow stress, i.e., independent of temperature and strain rate. Therefore, the differences of the plastic flow stress predicted by the proposed two bcc definitions emerge only in the athermal component. These differences may be attributed to both the errors accumulated using the nonlinear least-square fit and to the different integration results used in calculating the adiabatic heat accumulated inside the material through the plastic work. Therefore, the predicted stress-strain curves using the proposed bcc models will depend totally on the accuracy of determining the hardening parameters which vary from test to test. Moreover, the hardening parameters obtained using certain experimental data will not necessarily match with the other data set presented by different researchers.

Table 1. The proposed bcc models parameters for niobium, vanadium, and tantalum.

Model Parameters	Nb	V	Ta
Y_a (MPa)	60	60	50
$\bar{B}$ (MPa)	415	275	290
B (MPa)	450	305	330
n	0.25	0.16	0.41
ka	3.7	9.9	2.5
$\hat{\sigma}$ (MPa)	1350	945	1125
C_1	0.25	0.1	0.5
β_2 (K^{-1})	0.000149	0.0001392	0.0000937
$\dot{\varepsilon}_{po}^{i}$ (s^{-1})	7.07×10^6	6.32×10^6	4.45×10^6
q	3/2	3/2	3/2
p	1/2	1/2	1/2

Figures 4 and 5 show the adiabatic stress strain results for niobium computed using the present two bcc models at 3300 s^{-1} and 8000 s^{-1} strain rates respectively. Generally, both the proposed bcc definitions show very good agreement as compared to the experimental data presented by NEMAT-NASSER and GUO [44, 45] for a wide range of elevated temperatures. In fact, the difference in the predictions between the two proposed bcc relations for the plastic flow stress is noticeable at low strains (up to 0.1) and it diminishes with strain increase (up to 0.6).
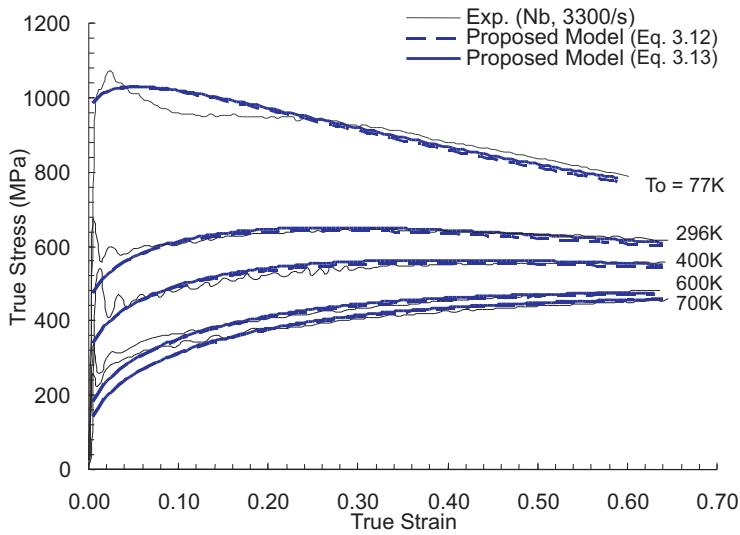
FIG. 4. Adiabatic flow stress of niobium predicted using the proposed models and compared to experimental results (NEMAT-NASSER and GUO, [44, 45]) at 3300 s^{-1} strain rate and indicated initial temperatures.
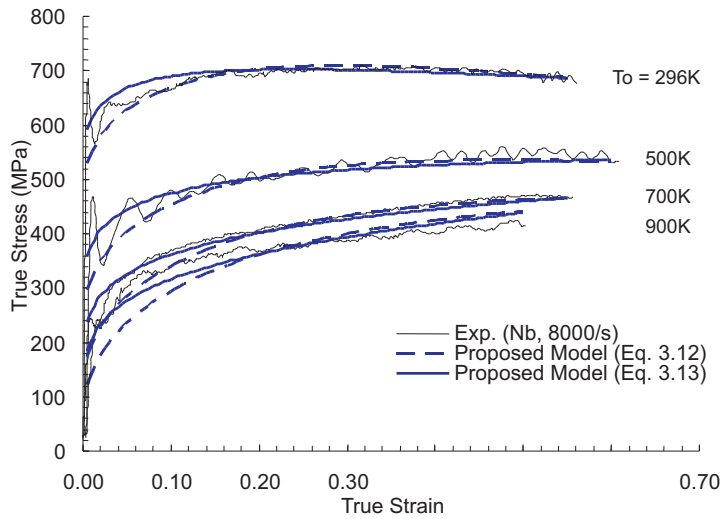
FIG. 5. Adiabatic flow stress of niobium predicted using the proposed models and compared to experimental results (NEMAT-NASSER and GUO, [44, 45]) at 8000 s^{-1} strain rate and indicated initial temperatures.

The experimental comparison of the adiabatic flow stress for the case of vanadium agrees well at the strain rate of 2500 s^{-1} and for different temperatures (up to 800 K) as shown in Fig. 6. The agreement, however, is less for the case of higher strain rate (8000 s^{-1}) with a temperature range of 296 K to 700 K

(see Fig. 7). This may indicate that assuming a constant value of the parameter k_a (i.e., neglecting the effect of temperature and strain rate) produces inaccurate results in some cases. Furthermore, the prediction of the adiabatic flow stress at different initial temperatures shows more variation between the two proposed bcc relations for the case of a strain rate of 8000 s^{-1} than those obtained at 2500 s^{-1} strain rate.
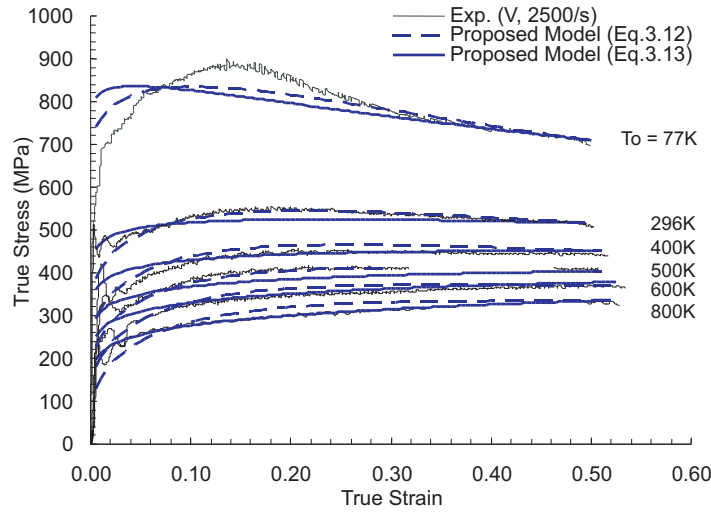
Fig. 6. Adiabatic flow stress of vanadium predicted using the proposed models and compared to experimental results (Nemat-Nasser and Guo [44–45]) at 2500 s^{-1} strain rate and indicated initial temperatures.
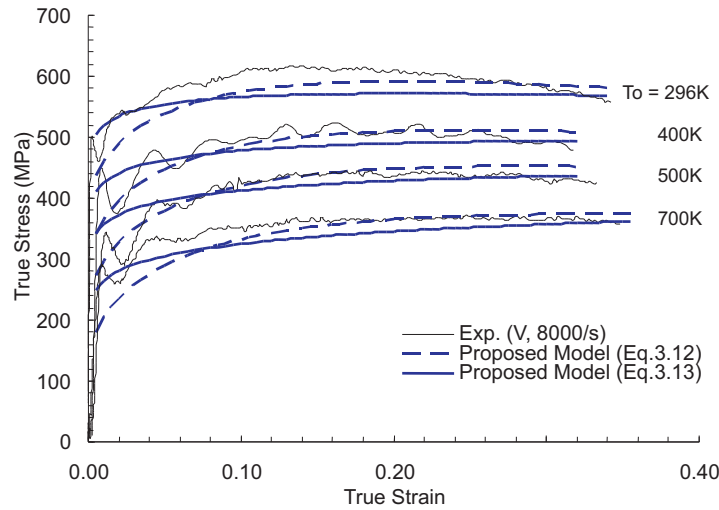
Fig. 7. Adiabatic flow stress of vanadium predicted using the proposed models and compared to experimental results (Nemat-Nasser and Guo [44–45]) at 2500 s^{-1} strain rate and indicated initial temperatures.

For the case of tantalum, Eq. (3.12) and Eq. (3.13) show almost identical results when computed at 5000 s^{-1} and temperature range of 298 K to 796 K. In addition, the adiabatic stress strain curves calculated by those two relations show good correlations with the experimental results provided by NEMAT-NASSER and ISAACS [41] as shown in Fig. 8.
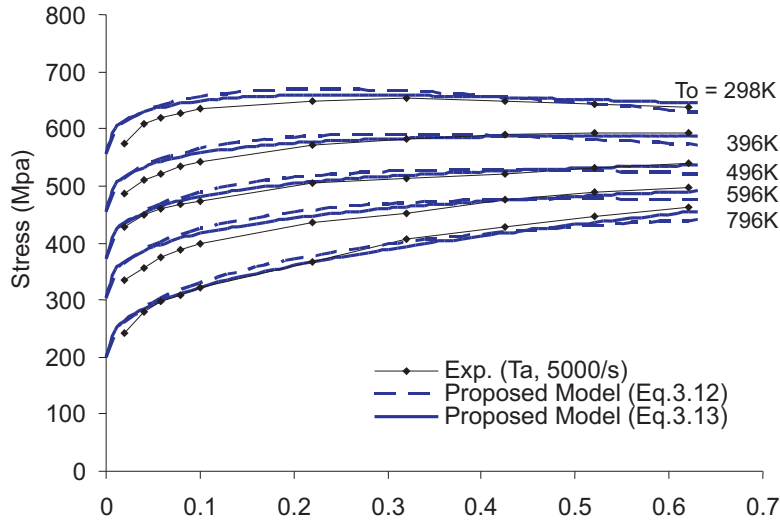
FIG. 8. Adiabatic flow stress of tantalum predicted using the proposed models and compared to experimental results (NEMAT-NASSER and ISAACS [41]) at 5000 s^{-1} strain rate and indicated initial temperatures.

The results of the model simulations from the above experimental data are also compared with other sets of experimental data. Fig. 9 shows the temperature variation of the flow stresses obtained experimentally by NEMAT-NASSER and ISAACS [47] at 0.05 strain and 5000 s^{-1} strain rate, HOGE and MUKHARJEE [18] at 0.014 strain and 0.0001 s^{-1} strain rate and BECHTOLD [10] at 0.014 strain and 0.00028 s^{-1} strain rate as compared with those calculated using the proposed model (Eq. (3.13)).

The proposed model, with the parameters obtained using the Nemat-Nasser and Isaacs data, predicts results that agree very well with the data given by Hoge and Mukharjee. The parameter Y_a, however, is changed to 133 MPa in order to get a better agreement with BECHTOLD [10] data. This change is used to allow for possible differences in solute and grain size effects.

Furthermore, the stress variation with strain rates computed using the proposed model Eq. (3.13), are compared with the experimental data presented by HOGE and MUKHARJEE [18] at room temperature and with the single crystal data obtained by MITCHELL and SPITIZIG [36] at 373° K temperature and MORDIKE and RUDOLPH [37] at 200° K temperature. The comparisons illustrated in Fig. 10 show very good agreement with the experimental results.
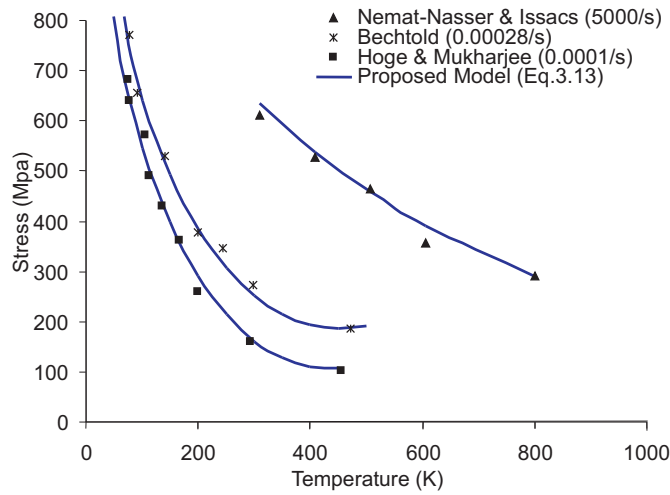
FIG. 9. Proposed model results of the temperature variation of the flow stress, for tantalum Ta, as compared to experimental data obtained by several authors at different strain rates.
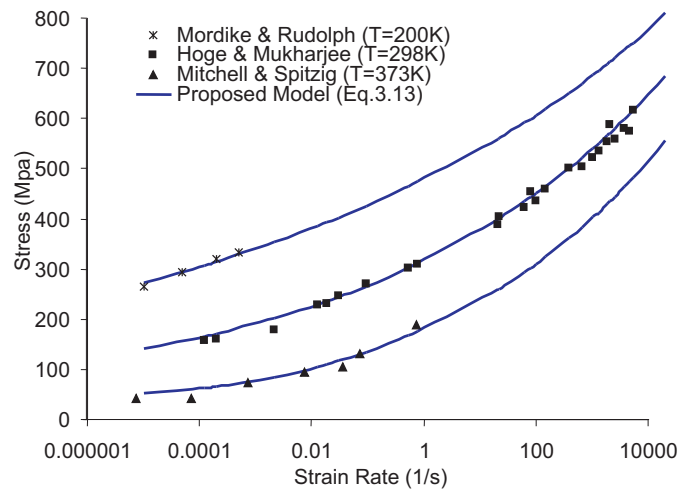
FIG. 10. Proposed model results of the strain rate variation of the flow stress, for tantalum Ta, as compared to experimental data obtained by several authors at different temperatures.

The adiabatic stress-strain curves of the plastically deformed specimens presented here are estimated using Eq. (3.14) where the thermo-mechanical parameters are listed in Table 2 for all metals used in this study. The incremental accumulation of the temperature during the adiabatic process is calculated by assuming a conversion of 100% plastic work into heat is used for Nb, V and Ta based on experimental results presented by NEMAT-NASSER and GUO [44, 45] and NEMAT-NASSER and ISAACS [41].

Table 2. **Thermal and Elastic properties for niobium, vanadium, tantalum, OFHC copper and titanium.**

Physical parameters	Nb	V	Ta	OFHC Cu	Ti
ρ (g/cm^3)	8.57	6.16	16.62	8.96	4.54
c_p (J/g.K)	0.265	0.498	0.139	0.383	0.523
ζ	1.0	1.0	1.0	0.9	1.0
μ (GPa)	37.0	45.0	60.0	45.0	43.0
μ_o (GPa)	70.0	75.0	90.0	77.0	75.0

4.2.2. Fcc metals. The Oxygen-Free High Conductivity (OFHC) copper is used here as an application for the proposed fcc models to show the temperature and strain rate variation of the flow stress. OFHC Cu is an important fcc metal used in the industry due to its high thermal and electrical conductivity and high ductility combined with low volatility which makes this material indispensable in the electronics industry. The material parameters of the proposed two fcc relations (Eq. (3.21) and Eq. (3.27)) are listed in Table 3 which are determined by following the same procedure explained in the previous section using the experimental data presented by Nemat-Nasser and Li [42]. Using the same parameters, the proposed fcc models are further compared to other experimental data found in the paper by Johnson and Cook [22].

Table 3. **The proposed fcc models parameters for OFHC copper.**

Model Parameters	OFHC Cu
Y_a (MPa)	25
$\hat{B}$(MPa)	1175
$\tilde{B}$(MPa)	990
Y_d or $\hat{Y}_d$ (MPa)	50
k_a	0.9
C_1	40
β_2 (K^{-1})	0.0000351
$\dot{\varepsilon}_{po}^i$ (s^{-1})	6.97×10^6
q	3/2
p	1/2

Generally, the adiabatic flow stresses calculated using the proposed fcc relations agree well with most of the experimental data for several strain rates and initial testing temperature. In Fig. 11, the adiabatic stress-strain calculated using both relations Eq. (3.21) and Eq. (3.27) predict very good results as compared with the Nemat-Nasser and Li [42] experimental data at 4000 s^{-1} strain rate and different initial temperatures (77 K–996 K). Equation (3.27), however, estimates higher stress values than those calculated by Eq. (3.21) at strains up to 0.45. These differences are generally ascribed to the two different definitions

used in calculating the hardening stresses. The flow stresses predicted by the proposed fcc relations are further compared to the experimental results conducted by the same authors at lower and higher strain rates (0.1 s^{-1} and 8000 s^{-1}) as shown in Fig. 12. The comparison shows good agreement as well.
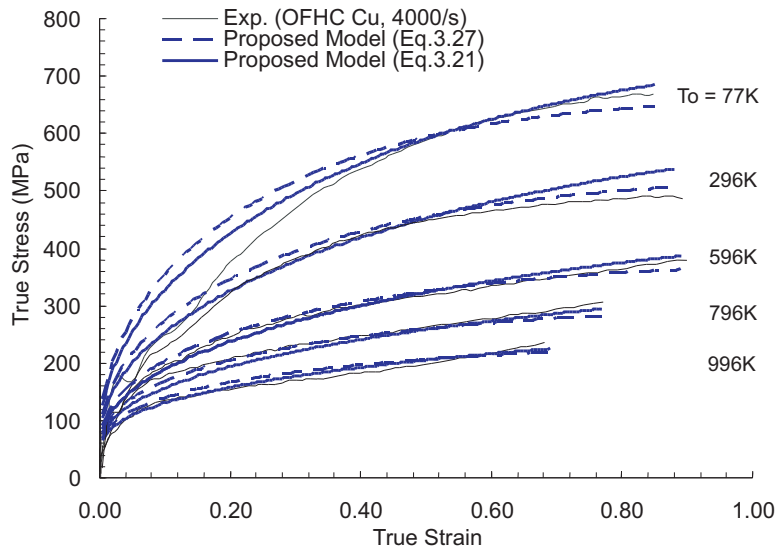
FIG. 11. Adiabatic flow stress of OFHC copper predicted using the proposed models and compared to experimental results (NEMAT-NASSER and LI [42]) at 4000 s^{-1} strain rate and indicated initial temperatures.
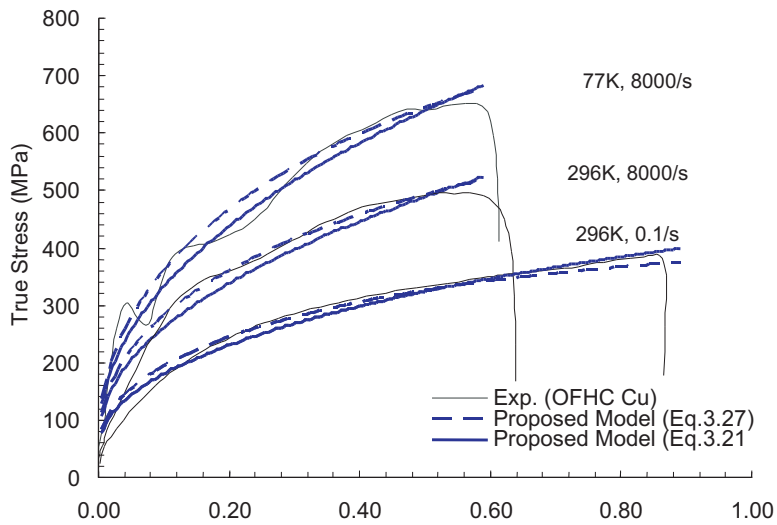
FIG. 12. Flow stress of OFHC copper predicted using the proposed models and compared to experimental results (NEMAT-NASSER and LI [42]) at strain rates of 8000 s^{-1} (adiabatic) and 0.1 s^{-1} (isothermal) and indicated temperatures.

An assessment of the model parameters determined using the experimental data by Nemat-Nasser and Li [42] can be made by comparing the adiabatic stress-strain results with the experimental data found in the paper of Johnson and Cook [22] as shown in Fig. 13. Overall, the predicted results of Eq. (3.21) correlate well with the experimental data at strain rates of 451 s^{-1}, 449 s^{-1} and 464 s^{-1} with initial temperatures of 298 K, 493 K and 730 K respectively. However, Eq. (3.27) overestimates the stress values in most cases. This deviation, however, is part due to neglecting the temperature and strain rate effects of the parameter k_a.
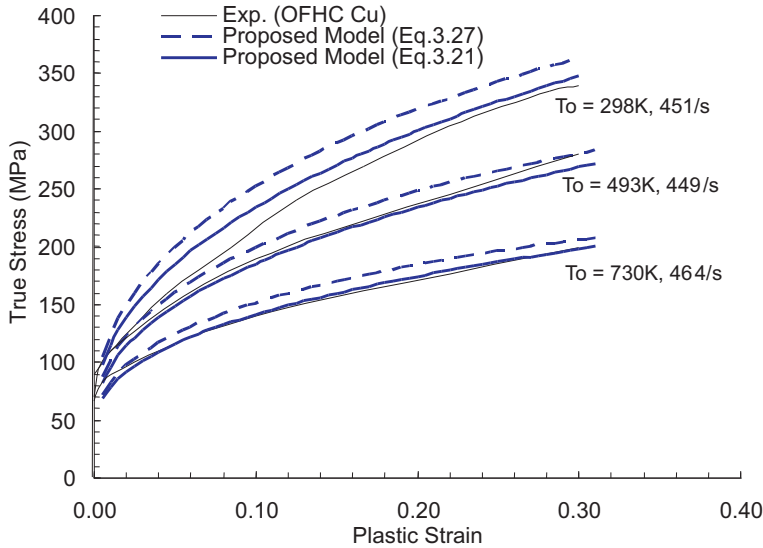
Fig. 13. Adiabatic flow stress of OFHC copper predicted using the proposed models and compared to experimental results (Johnson and Cook, [22]) at different strain rates of and temperatures.

In the case of copper, the prediction of the adiabatic stress strain curves predicted by the present model is obtained based on the assumption of conversion of 90% of the plastic work deformation to heat calculated using the same relation defined in Eq. (3.14) with the thermo-mechanical parameters listed in Table 2.

4.2.3. Hcp metals. The hcp commercially pure titanium (Cp Ti) used in this study has an axial ratio of c/a = 1.587, and is strongly plastically anisotropic as indicated by Nemat-Nasser *et al.* [43] who conducted both adiabatic and isothermal testing on both annealed and as received samples at low and high strain rates and temperatures. The experimental results clearly show that this material (Ti) is widely affected by the dynamic strain aging phenomenon over most strain rates and temperatures. At strain rates of 0.001 s^{-1} and 0.1 s^{-1}, the DSA effect starts clearly at temperature values of 296 K up to 500 K continuing

slightly up to 600 K for the case of isothermal process. At higher strain rates with adiabatic deformation (2200 s^{-1} and 8000 s^{-1} strain rates), the appearance of the DSA effects starts at 400 K temperature continuing up to 1000 K temperature.

As mentioned earlier, the proposed hcp models (Eq. (3.30) and Eq. (3.31)), which did not take into consideration the dynamic strain aging effects, are possibly not accurate in predicting both the adiabatic and the isothermal flow stresses in the strain rate and temperature ranges where the DSA effects are active. This indicates that the flow stresses predicted by the proposed two hcp relations will more likely underestimate the experimental results in theses ranges. The proposed model parameters for titanium are determined using the experimental data presented by NEMAT-NASSER *et al.* [43] using a combination of the bcc and fcc procedures described earlier. These parameters are listed in Table 4. In fact, the proposed hcp model is derived based on the fact that the plastic deformation behavior of most hcp metals shows a combination of both bcc and fcc plastic deformation behaviors.

Table 4. **The proposed hcp model parameters for titanium.**

Model Parameters	Ti
Y_a (MPa)	20
$\hat{B}$ (MPa)	2050
$\tilde{B}$ (MPa)	2025
Y_d or $\hat{Y}_d$ (MPa)	115
ka	1.31
C_1	0.9
β_2 (K^{-1})	0.0000433
$\dot{\varepsilon}_{po}^i$ (s^{-1})	1.95×10^7
q	3/2
p	1/2
$\bar{B}$ (MPa)	90
B (MPa)	85
n	0.43

Next, assessments of the proposed hcp models are made by comparing the isothermal stresses predicted using both Eq. (3.30) and Eq. (3.31) to the experimental results by NEMAT-NASSER *et al.* [43] at 0.001s strain rate and different temperatures as shown in Fig. 14. The comparison between the predicted results and the experimental data shows good agreement at temperature values of 77 K, 673 K and 773 K whereas they underestimate the experimental results at other temperatures due to the effect of DSA. In Fig. 15, the adiabatic stress-strain results predicted by the proposed hcp models are compared to the experimental data at a strain rate of 2200 s^{-1} and different initial temperatures. Similarly, the comparison agrees well at temperatures where the DSA is inactive (77 K and 296 K) whereas, the proposed models predict lower results at temperatures where the DSA effect is dominating.
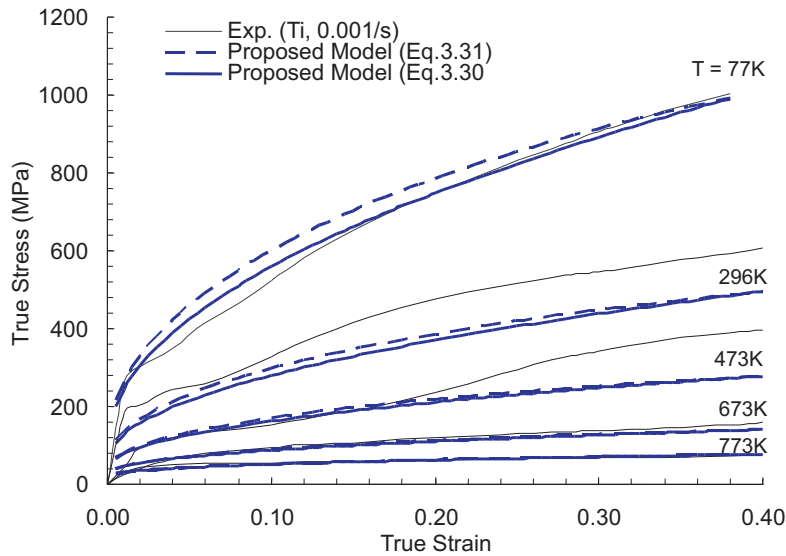
FIG. 14. Isothermal flow stress of titanium predicted using the proposed models and compared to experimental results (NEMAT-NASSER *et al.* [43]) at 0.001 s^{-1} strain rate and indicated temperatures.
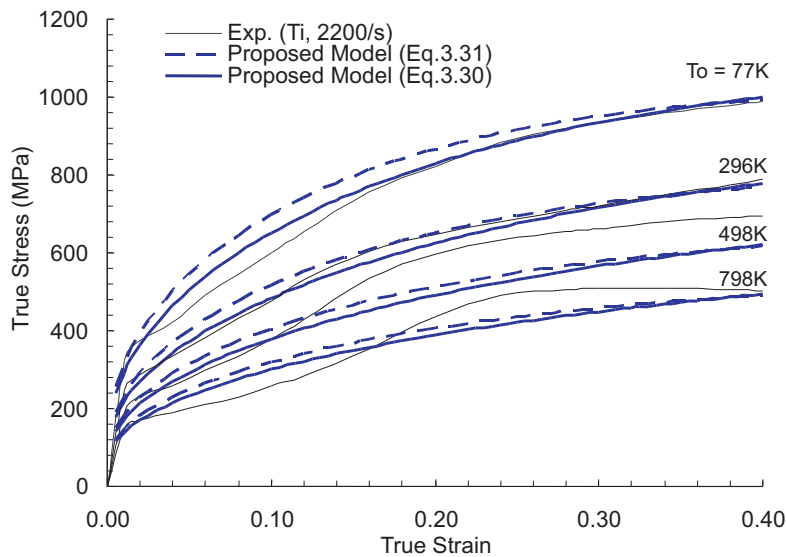
FIG. 15. Adiabatic flow stress of titanium predicted using the proposed models and compared to experimental results (NEMAT-NASSER *et al.* [43]) at 2200 s^{-1} strain rate and indicated initial temperatures.

The flow stress prediction of the proposed hcp models are further compared to the experimental results at the strain rate of 0.1 s^{-1} for the case of isothermal

deformation process and at the 8000 s^{-1} strain rate for the case of adiabatic deformation as shown in Fig. 16. Similar comparison results are concluded for both strain rates. In comparing the flow stress results predicted by the proposed two hcp relations, it is found that Eq. (3.31) deviates largely at higher strain rates predicting higher stress values than those calculated using Eq. (3.30). This deviation, however, appears noticeably at strain values up to 30%.
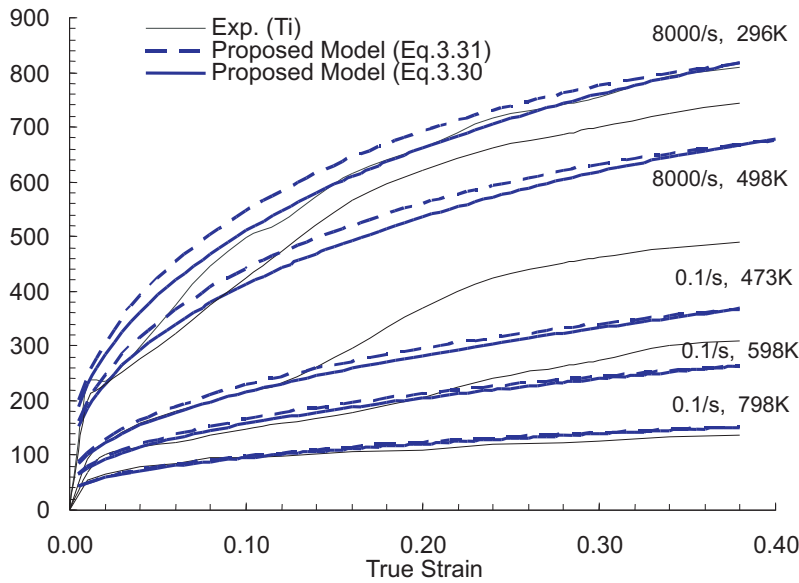
Fig. 16. Flow stress of titanium predicted using the proposed models and compared to experimental results (Nemat-Nasser *et al.* [43]) at strain rates of 0.01 s^{-1} (isothermal) and 8000 s^{-1} (adiabatic) and indicated temperatures.

For the case of titanium, a 100% of the plastic work generated during the deformation process under different strain rates is converted to heat as given by Nemat-Nasser *et al.* [43]. The temperature accumulation during the plastic deformation is, therefore, calculated using Eq. (3.14) with the thermo-mechanical parameters for Ti given in Table 2.

4.3. Discussions

In investigating the proposed bcc, fcc and hcp models, the definition of the thermal component of the flow stress is nearly the same for all kinds of metals. However, the model parameters values and accordingly the physical quantities differ from metal to metal. In addition, it is found that the thermal stress for all bcc metals used in this study is independent of strain. That is to say, the effect of the parameter β_1 which represents the effect of the evolution of the

mobile dislocation density that is thermally affected through Orowan's equation is almost negligible. This, however, supports the experimental observations which indicate that the thermal stresses for most bcc metals are strain-independent and mainly controlled by the yield stress. This behavior can be interpreted physically as the resistance of the initial dislocation motion by the Peierls barriers. On the other hand, the thermal component of the flow stress for fcc metals depends mainly on the strain through the evolution of the mobile dislocation density defined by the parameter β_1 and also through the evolution of the remaining part (mainly forest) of the dislocation density introduced through the hardening parameters definitions given by Eq. (3.22) or Eq. (3.28). For the case of hcp metals, the strain dependence of the thermal stresses is introduced only through the hardening parameters, whereas the effect of β_1 is very small and can be neglected. Figure 17 shows the thermal component of the flow stresses as varying with the plastic strain using the proposed models for V, Nb, Ta, Ti and OFHC Cu at strain rate and temperature values of 8000 s^{-1} and 296 K respectively.
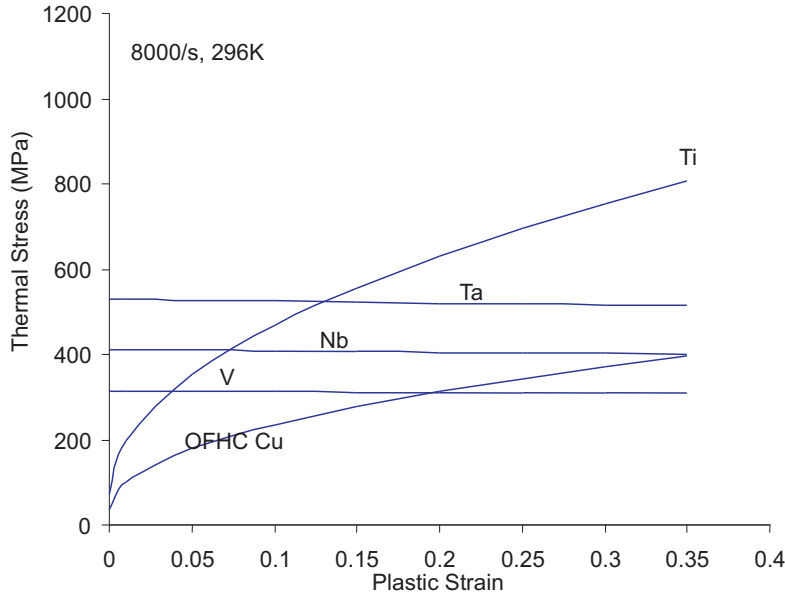
FIG. 17. Strain variations of the thermal stresses for several metals using the proposed models at 8000 s^{-1} strain rate and 296 K° temperature.

The consequence of the variation of the parameter β_1 with plastic strain for fcc metals is observed in determining the values of the critical temperature (T_{cr}) that become strain-dependent as well. In contrast, the critical temperature for bcc and hcp metals does not depend on plastic strain. In fact, T_{cr} is defined as the highest temperature value that corresponds to the minimum thermal stresses (zero thermal stress) observed during the degradation process of the

flow stress as the material temperature increases. Figure 18 shows the strain rate variation of T_{cr} calculated using Eq. 3.14 for the five metals used in this study at 0.1 plastic strain. It is found that T_{cr} values increase with strain rates increase. Also, the critical temperature values for OFHC Cu and Ti are higher than those obtained for the three bcc metals. This disparity may be attributed to the variation of the reference plastic strain rate $\dot{\varepsilon}_{po}^{i}$ values and also to the different β_2 values that is mainly related to the Gibbs free energy G_o. Since $\dot{\varepsilon}_{po}^{i}$ values for all metals used in this study are approximately of the same order, the value of G_o is considered the major factor that affects the variation of T_{cr} values from one metal to another at a fixed strain rate. The higher the activation energy values (around 2.4, 2.0, 0.92, 0.62, 0.58 eV/atom for Cu, Ti, Ta, V, and Nb respectively) needed to overcome the barriers, the higher the critical temperature values achieved. Actually, the thermal stress is interpreted as the resistance of the barriers to the dislocation movement, thus, the barriers that need higher activation energy to be overcome require also higher temperature to produce this thermal energy until the resistance of these barriers has vanished which indicates zero thermal stresses.
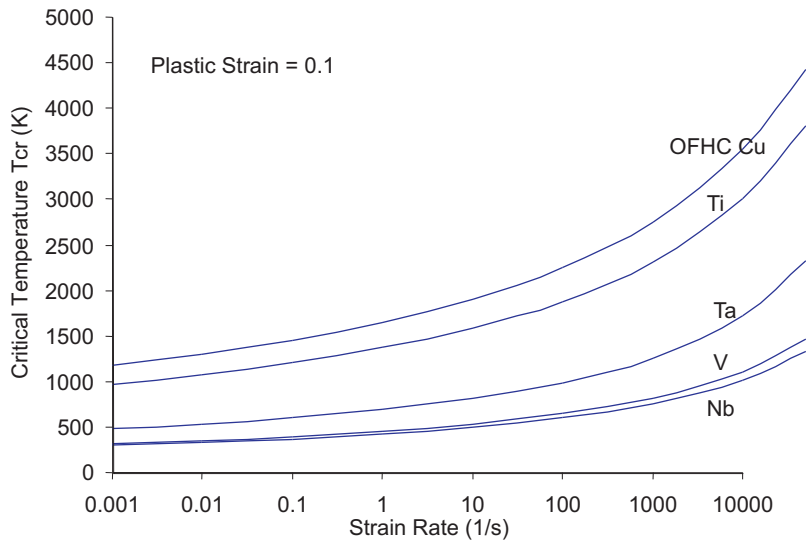
FIG. 18. Critical temperatures predicted by the proposed models for several metals at 10% strain and different strain rates.

In general, most metals contain initial amount of dislocations which are naturally excited or generated through the manufacture process. These dislocation densities, however, help metals to deform plastically until a level where no further dislocations generation are allowed, which indicates that the saturation limit of dislocation densities is reached. The initial and saturated values of the dislo-

cation densities, however, differ from metal to metal. The numerical values of the physical nano- and micro-quantities used in defining the proposed models that are obtained for the indicated metals are listed in Table 5. Although these quantities are defined based on the model parameters that are fitted experimentally, their values are found to be reasonable when compared to those available in the literature. The initial dislocation density values are fixed and set around 5×10^{12} m^{-2} for the case of bcc metals and little higher for fcc and hcp metals. Consequently, the saturated values of these dislocation densities are found to be of the order of 10^{15} m^{-2} for all metals. In fact, the effect of initial dislocation density enters the proposed models through the thermal component of the flow stress. This effect, however, is expected to be higher for bcc metals than other metal structures due to the fact that the thermal stress of bcc metals is nearly related to the yield stress (Peierls stress) and not affected by the dislocation density evolution with plastic strain. That is to say, the yielding strength is less when the material contains high initial dislocation density and *vice versa*. Once the material yields, the evolution of dislocation density along with the initial dislocation density contribution plays a crucial role in determining the flow stress and particularly the thermal stress as in the case for most fcc metals and slightly less for hcp metals. Figure 19 shows, for all metals presented here, the variation effect of initial dislocation density generated inside the material on the flow stress at 298 K and 8000 s^{-1} temperature and strain rate'respectively. It is obvious that the flow stress decreases with the increase of the originated (initial) dislocation density. The decreasing slopes for bcc metals are higher than those for hcp and fcc metals which supports the above-mentioned argument.

Table 5. Numerical values for the physical quantities used in deriving the proposed models parameters for Nb, V, Ta, OFHC Cu and Ti.

Physical parameters	Nb	V	Ta	OFHC Cu	Ti
G_o (eV/atom)	0.58	0.62	0.92	2.4	2.0
b (Å)	3.3	3.1	2.9	2.5	3.0
v_o (m/sec)	8.57×10^3	8.3×10^3	7.71×10^3	3.97×10^3	5.1×10^3
ρ_{mi} (m^{-2})	5×10^{12}	4.9×10^{12}	4.1×10^{12}	1.4×10^{13}	2.55×10^{13}
ρ_{fi} (m^{-2})	2×10^{12}	2×10^{12}	2×10^{12}	1.1×10^{13}	2.69×10^{13}
ρ_s (m^{-2})	4.5×10^{15}	1.5×10^{15}	1.1×10^{15}	6.1×10^{15}	9.0×10^{15}
A_o (m^2)	26b^2	27b^2	27b^2	–	–
D_g (mm)	0.013	0.016	0.0375	0.073	0.125
A'_o (m^2)	–	–	–	585b^2	321b^2
A''_o (m^2)	–	–	–	30b^2	18b^2

It is interesting to note that the Helmholtz free energy values for fcc metals are higher than those found for bcc metals which indicates that the dislocation interaction mechanism necessitates higher activation energy than the Peierls mech-
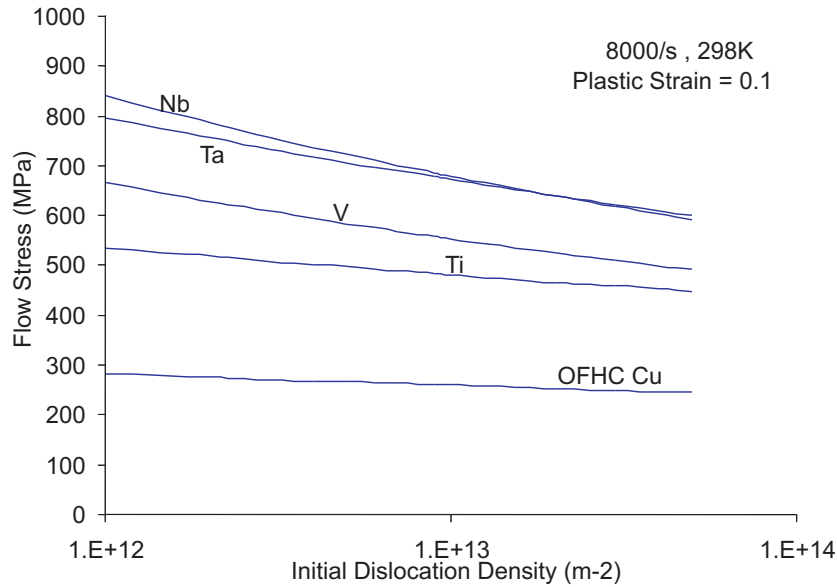
FIG. 19. Initial dislocation density variation of the flow stress, for several metals, computed at 8000 s^{-1} strain rate and 298 K° temperature.

anism in overcoming the short-range barriers. Consequently, the waiting time needed by the dislocation to overcome an obstacle is less for bcc $[t_w = O(10^{-12} \text{ s})]$ than those required for fcc metals $[t_w = O(10^{-11} \text{ s})]$ (KOCKS *et al.* [28]). Therefore, the reference velocity $v_o = d \sim b/t_w$ values of fcc metals are less than the ones obtained for bcc metals as illustrated in Table 5. Moreover, the average values of the Burger vector are chosen to be around 3.3, 3.1, 2.9, 2.5 and 3.0Å for Nb, V, Ta, OFHC Cu and Ti respectively.

In the proposed models, the following typical values of 1.5 and 0.5 for the exponents p and q respectively are used for all metals. Unfortunately, the value of $\hat{\sigma}$ in the thermal component of the bcc flow stress is sensitive to the choice of p which characterizes the tail of the obstacle. This sensitivity, however, is less for the case of fcc and hcp metals in obtaining the parameters and Y_d. In fact, $\hat{\sigma}$ represents a parameter which refers to a state of zero Kelvin temperature. It should be noted here that the determination procedure of the proposed bcc, fcc and hcp model parameters is simple and straightforward. However, more caution is required in the numerical techniques used in obtaining the hardening parameters that produce not only the hardening stresses but also the temperature evolving with the plastic work.

In the proposed model, two different definitions for the hardening stresses are presented. The first definition is derived based on experimental observations which indicate that the fitting of the hardening stresses can be achieved using

the power law definition. On the other hand, the second definition of the hardening parameters is derived using the concept of dislocation density evolution with plastic strain. Both definitions are used in predicting the isothermal and adiabatic flow stresses and compared with the available experimental data. It is found that the power-law definition of the plastic hardening stresses predicts more accurate results than the other definition in most experimental comparisons at different strain rates and temperatures. Actually, the deviation of the predicted results may be attributed to the use of constant values for the parameter k_a assumed in the derivation of the proposed model.

For the bcc metals presented here, it is found that the dynamic strain aging activates when the temperature reaches its critical values. In this stage, dislocations require higher temperatures to overcome the obstacle which consequently increases the waiting time of these dislocations before the obstacle. This, in turn, helps in activating the dynamic strain aging by strengthening the obstacles through the diffusion process of the atoms and accordingly, increasing suddenly the flow stress throughout the deformation process. On the other hand, the dynamic strain aging effect is observed in titanium over a wide range of temperatures and at all strain rates. It is found that the DSA phenomenon activates at different temperature depending on the strain rate values. These temperature values increase as the strain rates increase. In the case of OFHC copper, however, the dynamic strain aging is not observed for most of the strain rates and temperatures used in the presented experimental comparisons. The effect of DSA on the plastic flow simulation along with the strain rate and temperature dependence of the dislocation annihilation factor k_a will be discussed in a forthcoming paper by the authors.

5. Conclusions

The effect of dislocation density evolution with plastic strain is incorporated in modeling the thermo-mechanical response of different structure types of metals. The proposed models are derived basing on the concept of thermal activation energy as well as the dislocation interaction mechanisms. Two different definitions for modeling the hardening stresses are employed using the least-square technique. The first definition uses the experimental power law fitting, whereas the second one is derived using the plastic strain evolution of the dislocation density. The simulation of the adiabatic and isothermal plastic flow stresses for different bcc, fcc and hcp metals is achieved at low and high strain rates and temperatures. The predicted results, generally, show good agreement as compared with different experimental results conducted by several authors for niobium, vanadium and tantalum for bcc metals, titanium for hcp metal and OFHC copper for fcc metal.

In bcc metals, the thermal yield stress, due to the short-range barriers (Peierls barriers), shows strong dependence on the strain rate and temperature while the plastic strain hardening which represents the athermal stress is independent of them. On the contrary, the thermal stress in fcc metals is strongly dependent on the plastic strain due to domination of the dislocation intersections on the mechanisms behavior of the thermal activation analysis. For the case of hcp metals, the thermo-mechanical behavior shows a combination between the plastic deformation behavior of both bcc and fcc structures. Thus, the thermal component as well as the athermal component of the flow stress for the proposed hcp model strongly depends on the plastic strain. Besides, both yielding and hardening stresses are strain rate and temperature-dependent.

The dynamic strain aging phenomenon is clearly encountered in titanium for most temperatures and strain rates while it activates only at low strain rates and over a narrow range of high temperatures for most bcc metals. For OFHC copper, the DSA effect is not observed for the present temperature and strain rate range of experimental data. In fact, the dynamic strain aging encountered in some metals at certain temperatures is strain rate dependent. Its effect, however, is not included in the present modeling where the dislocation movement as well as the dislocation evolution controls the plastic deformation in the absence of diffusion and creep.

It is concluded from the stress-strain prediction of the proposed bcc models that the effect of the parameter β_1 which represents the evolution of the thermally affected part of the mobile dislocation density is almost negligible. That is the evolution of the mobile and forest dislocation density is related to the athermal part of the flow stress. In contrast, the mobile dislocation density evolution through the parameter β_1 as well as the forest dislocation density evolution through the hardening parameters shows considerable dependence on the thermal stresses of OFHC copper. In titanium, on the other hand, the effect of β_1 on the thermal stresses is very small which indicates that the strain dependence of the thermal stresses is ascribed to the hardening stress that is mainly generated through the evolution of the forest dislocation density.

Acknowledgment

References

1. Abed, F.H., Voyiadjis, G.Z., *Plastic deformation modeling of AL-6XN stainless steel at low and high strain rates and temperatures using a combination of bcc and fcc mechanisms of metals*, Accepted in International Journal of Plasticity, **21**, 1618–1639, 2004.

2. Aifantis, E.C., *The physics of the plastic deformation*, International Journal of Plasticity, **3**, 211–247, 1987.

3. Ashby, M.F., *The deformation of plasticity non-homogenous alloys*, Philosophical Magazine **21**, 399–424, 1970.

4. Ashby, M.F., Frost, H.J., *The Kinematics of inelastic deformation above 0K^o*, [in:] Argon, A.S. [Ed.], Constitutive Equations of Plasticity., 117, 1975.

5. Armstrong, R.W., Ramachandran, V., Zerilli, F.J.,[in:] *Materials for Advanced Technology System*, Indian Institute of Metals Symposium, India 1993.

6. Bammann, D.J., Aifantis, E.C., *On a proposal of continuum with microstructure*, Acta Mechanica **45**, 91–125, 1982.

7. Bammann, D.J., Aifantis, E.C., *A model for finite-deformation plasticity*, Acta Mechanica **69**, 97–117, 1987.

8. Bammann, D.J., *A model of crystal plasticity containing a natural length scale*, Material Sciences and Engineering A309–310, 406–410, 2001.

9. Barlat, F., Glazov, M.V., Brem, J.C., Lege, D.J., *A simple model for dislocation behavior, strain and strain rate hardening evolution in deforming aluminum alloys*, International journal of Plasticity, **18**, 919–939, 2002.

10. Bechtold, J.H., Acta Metallurgica. **3**, 249, 1955.

11. Bell, J.F., *Crystal plasticity*, Philosophical Magazine **11**, 1135–1145, 1965.

12. Cheng, J., Nemat-Nasser, S., *A model for experimentally-observed high strain rate dynamic strain aging in titanium*, Acta Materialia. **48**, 3131–3144, 2000.

13. Chichili, D., Ramesh, K., Hemker, K., *The high-strain response of Alpha titanium: experimental, deformation mechanisms and modeling*, Acta Materialia. **46**, 1025–1043, 1998.

14. Christian, J.W., *Some surprising features of the plastic deformation of body-centered cubic metals and alloys*, Metallurgical Transactions **A14**, 1237–1256, 1983.

15. Follansbee, P.S., Regazzoni, G., Kocks, U.F., *Transition to drag-controlled deformation in copper at high strain rates*, Institute of Physics Conference Series. **70**, 71–80, 1984.

16. Friedel, J., *Dislocations*, Pergamon Press Oxford 1964.

17. Hirth, J.P., Nix, W.D., *An analysis of the thermodynamics of dislocation glide*, Physica Status Solidi. **35**, 177–188, 1969.

18. Hoge, K., Mukhejee, K., *The temperature and strain rate dependence of the flow stress of tantalum*, Journal of Material Science. **12**, 1666–1672, 1977.

19. Gillis, P.P., Gilman, J.J., *Dynamical dislocation theory of crystal plasticity*, Journal of Applied Physics. **36**, 3370–3380, 1965.

20. Gracio, J.J., *Effect of grain size on substructural evolution and plastic behavior of copper*, Material Science and Engineering, **A118**, 97–105, 1989.

21. Jassby, K.M., Vreeland, T., *An experimental study of mobility of edge dislocations in pure copper single crystals*, Philosophical Magazine **21**, 1147–1159, 1970.

22. Johnson, G., Cook, W., *Fracture characteristics of three metals subjected to various strains, strain rates, temperatures and pressures*, Engineering Fracture Mechanics. **21**, 31–48, 1988.

23. Kapoor, R. and Nemat-Nasser, S., *Determination of temperature rise during high strain rate deformation*, Mechanics of Materials. **27**, 1–12, 1998.

24. Kelly, J.M., Gillis, P.P., *Continuum descriptions of dislocations under stress reversals*, Journal of Applied Physics. **45**, 1091–1096, 1974.

25. Klepaczko, J.R., *Modeling of structural evolution at medium and high strain rates, FCC and BCC metals*, [in:] Constitutive Relations and Their Physical Basis. Roskilde, Denmark 387–395, 1987.

26. Klepaczko, J.R., *A general approach to rate sensitivity and constitutive modelin of fcc and bcc metals*, In Impact Effects of Fast Transient Loading, A.A. Balkema, Rotterdam 3–10, 1988.

27. Klepaczko, J.R., Rezaig, B., *A numerical study of adiabatic shear bending in mild steel by dislocation mechanics based constitutive relations*, Mechanics of Materials, **24** 125–139, 1996.

28. Kocks, U.F., Argon, A.S., Ashby, M.F., *Thermodynamics and kinetics of slip*, Progress in Materials Science, 19, Pergamon, Oxford 1975.

29. Kocks, U.F., *Realistic constitutive relations for metal plasticity*, Material Science and Engineering, **A317**, 181–187, 2001.

30. Kubin, L.P., *Reviews on the Deformation Behavior of Materials*, **4**, 181–275, 1982.

31. Kubin, L.P., Estrin, Y., *Evolution for dislocation densities and the critical conditions for the Portevin-le Chatelier effect*, Acta Metallurgical Materialia, **38**, 697–708, 1990.

32. Kubin, L.P., Shihab, K., *The rate dependence of the Portevin-Le Chatelier effect*, Acta Metallurgica, **36**, 2707–2718, 1988.

33. Lennon, A.M., Ramesh, K.T., *The influence of crystal structure on the dynamic behavior of materials at high temperatures*, International journal of Plasticity, **20**, 269–290, 2004.

34. Li, J.C., *Kinetics and dynamics in dislocation plasticity*, Dislocation Dynamics, McGraw-Hill, 87–116, 1968.

35. Louat, N., *On the theory of the Portevin-Le Chatelier effect*, Scripta Metallurgica, **15**, 1167-1170, 1981.

36. Mitchel, T.E., Spitzig, W.A., *Three-stage hardening in tantalum single crystals*, Acta Metall., **13**, 1169–1179, 1965.

37. Mordike, B.L., Rudolph, G., *Three-stage hardening in tantalum deformed in compression* J. Mater. Sci., **2**, 332–338, 1967.

38. Nabarro, F.R.N., Basinski, Z.S., Holt, D.B., *The plasticity of pure single crystals*, Advances in Physics, **13**, 193–323, 1964.

39. Nadgornyi, E.M., *Dislocation dynamics and mechanical properties of crystals*, Progress in Materials Science, **31**, 473–510, 1988.

40. Nemat-Nasser, S. and Li, Y., *Flow Stress of F. C.C. Polycrystals with Application to OFHC Cu,*, Acta Materialia, **46** 565–577, 1998.

41. Nemat-Nasser, S., Isaacs, J., *Direct measurement of isothermal flow stress of metals at elevated temperatures and high strain rates with application to Ta and Ta-W alloys*, Acta Metallurgica, **45**, 907–919, 1997.

42. Nemat-Nasser, S. and Li, Y., *Flow Stress of F. C.C. Polycrystals with Application to OFHC Cu,* Acta Materialia, **46**, 565–577, 1998.

43. Nemat-Nasser, S., Guo, W., Cheng, J., *Mechanical properties and deformation mechanisms of a commercially pure titanium*, Acta Materialia, **47**, 3705–3720, 1999.

44. Nemat-Nasser, S. and Guo, W., *Flow stress of commercially pure niobium over a broad range of temperature and strain rates*, Material Science Engineering. **A284**, 202–210, 2000.

45. Nemat-Nasser, S. and Guo, W., *High strain rate response of commercially pure vanadium*, Mechanics of Materials **32**, 243–260, 2000.

46. Nemat-Nasser, S., Guo, W. and Kihl, D., *Thermomechanical response of AL-6XN stainless steel over a wide range of strain rates and temperatures*, Journal of Mechanics and Physics Solids, **49**, 1823–1846, 2001.

47. Orowan, E., Discussion in Symposium on internal stresses in metals and alloys. Institute of Metals, London, 451, 1948.

48. Rusinek, A. Klepaczko, J.R., *Shear testing of a sheet steel at wide range of strain rates and a constitutive relation with strain-rate and temperature dependence of the flow stress*, International Journal of Plasticity, **17**, 87–115, 2001.

49. Sackett, S.J., Kelly, J.M., Gillis, P.P., *A probabilistic approach to polycrystalline plasticity*, Journal of Franklin Institute, **304**, 33–63, 1977.

50. Stein, D.L., Low, J.R., *Mobility of edge dislocations in silico-iron crystals*, Journal of Applied Physics. **31**, 362–369, 1960.

51. Tanner, A., McGinty, R., McDowell, D., *Modeling temperature and strain rate history effects in OFHC Copper,* International Journal of Plasticity, **15**, 575–603, 1999.

52. Taylor, G.I.,*Plastic strain in metals*, Journal of Inst. Metals, **62**, 307–324, 1938.

53. Taylor, G., *Thermally-activated deformation of bcc metals and alloys*, Progress in Material Science, **36**, 29–61, 1992.

54. Vitek, V., Duesbury, M.S., *Plastic anisotropy in bcc transition metals*, Acta Materialia, **46**, 1481–1492, 1998.

55. Voyiadjis, G.Z., Abed, F.H., *Microstructural based models for bcc and fcc metal with temperature and strain rate dependency*, Mechanics of Materials, **37**, 355–378, 2005.

56. Vreeland, T., Jassby, K.M., *Temperature dependent viscous drag in close-packed metals*, Material Science and Engineering, **7**, 95–103, 1971.

57. Yoo, M.H., Morris, J.R., Ho, K.M., Agnew, S.R., *Nonbasal deformation modes of hcp metals and alloys: role of dislocation source and mobility*, Metallurgical Materialia Transaction, **33**, 813–822, 2002.

58. ZAISER, M., GLAZOV, M., LALLI, L.A., RICHMOND, O., *On the relations between strain and strain-rate softening phenomena in some metallic materials: a computational study*, Journal of Computational Material Science, **15**, 35–49, 1999.

59. ZERILLI, F.J., ARMSTRONG, R.W., *Dislocation-mechanics-based constitutive relations for material dynamics calculation*, Journal of Applied Physics, **5**, 1816–1825, 1987.

60. ZERILLI, F.J., ARMSTRONG, R.W., *The effect of dislocation drag on the stress-strain behavior of fcc metals*, Acta Metallurgical and Materialia, **40**, 1803–1808, 1992.

61. ZHAO, M., SLAUGHTER, W.S., LI, M., MAO, S.X., *Material-length-scale-controlled nano-indentation size effects due to strain gradient plasticity*, Acta Materialia, **51**, 4461–4469, 2003.